Doctoral Dissertation

Observation of lightning narrow bipolar event with LF lightning location systems and phased array radar

Ting Wu

January 2013

Graduate School of Engineering,
Osaka University

Doctoral Dissertation

Observation of lightning narrow bipolar event with LF lightning location systems and phased array radar

Ting Wu

January 2013

Graduate School of Engineering,
Osaka University

Preface

Lightning narrow bipolar event (NBE) is one of the most mysterious types of lightning discharge. Since its discovery in the 1980s, both ground-based and satellite-based observations have been carried out in many regions of the world. There have been numerous studies on its characteristics of waveform, radiation, physical mechanism and meteorological context. However, there are still many special characteristics of NBE that are difficult to understand, and many fundamental problems such as its production mechanism and relationship with thunderstorm are waiting to be answered. In this thesis, I will analyze characteristics of NBE from multiple respects based on observations with both LF lightning location system and phased array radar.

This thesis consists of seven chapters, organized as follows:

In Chapter 1, I introduce basic types and characteristics of lightning discharges and the general relationship between NBE and normal lightning. Then I review some important studies on NBE and summarize its general characteristics. At last, I present the objective and main contents of this thesis.

Chapter 2 introduces experiments, instrumentations and data for this study. There are four experiments in four different regions. LF lightning location system was built for each experiment. In the experiment in Osaka region, a phased array radar was utilized. General properties of the LF lightning location system and the phased array radar are presented.

Chapter 3 deals with waveform characteristics of NBE. First, large electric field changes produced by NBEs are analyzed. Peak magnitude of electric field changes produced by return strokes, positive and negative NBEs are compared with each other. It is found that NBEs generally produce larger electric field changes than return strokes do, and negative NBEs are more powerful than positive NBEs. Then the characteristic of temporal isolation of NBE is statistically analyzed. NBEs are usually found isolated with other discharge processes. However, some portion of NBEs can be the initiation processes of regular discharge processes, and in this case, positive NBEs have much higher possibility than negative NBEs. At last, characteristics of ionospheric reflection pairs of NBEs are analyzed. Ionospheric reflection pairs are formed when the LF radiation of NBE is reflected at the ionosphere and the ground. The arrival time and magnitude of these pulses are analyzed with a simple model.

Chapter 4 focuses on the discharge height of NBE. Discharge height is essential for understanding NBE because it determines position of NBE in a thunderstorm. I develop

a method to locate NBE using its ionospheric reflection pairs. This method is much more accurate than traditional TOA or interferometry techniques. With this method, discharge heights of thousands of both polarities of NBEs are computed, and it is found that positive NBEs mainly occur at the height of 7-15km, corresponding to the region between the main negative charge layer and the upper positive charge layer, while negative NBEs mainly occur at the height of 15-18km, corresponding to the region between the upper positive charge layer and the screening negative charge layer at the cloud top. Further, variation of NBE discharge height in two thunderstorms are analyzed, and it is found that for a given short time period in a single thunderstorm, negative NBEs are always observed to occur at a higher altitude than positive NBEs, indicating a dividing charge layer between positive NBEs and negative NBEs.

Chapter 5 focuses on the relationship between NBE and thunderstorm. First, a statistical study on the relationship is presented, confirming the general result that NBE rate increases with increasing convective strength. It is also found that the percentage of negative NBE seems to increase with increasing convective strength. In another word, as the thunderstorm grows more vigorous, it is more inclined to produce negative NBE. Based on the observation of phased array radar with unprecedented high temporal and spatial resolution, the spatial relationship between NBE and thunderstorm is analyzed. It is found that negative NBEs are usually located very close to the cloud top of thunderstorm; they can be either at the inner or the outer boundary of the cloud top. Positive NBEs, on the other hand, are always located well inside thundercloud. It seems that negative NBEs can only be produced in thunderstorms with cloud top higher than about 14 km. Numerous thunderstorms with lower height did not produce any negative NBE.

Chapter 6 discusses some major problems on NBE. First, I analyze the possibility of NBE production in winter thunderstorm based on our observation in Hokuriku region of Japan. Second, I put forward a hypothesis that NBEs can only be produced above certain height, that is, there is a height threshold for NBE production. Finally, I suggest a way to monitor severe thunderstorm with NBE.

Chapter 7 summarizes all the conclusions of this thesis.

Acknowledgement

I would like to take this chance to express my deep gratitude to all the people who have helped and supported me during my PhD study at Kawasaki Laboratory, Osaka University.

First I want to thank Prof. Zen Kawasaki, who gave me tremendous help for my researches. Numerous discussions with him have greatly broadened my perspective and inspired some important results. It would be impossible for me to finish this thesis in such short time without his help.

I am much indebted to Prof. Tsuyoshi Funaki, who helped me to make the best preparations for every major step through my study in Osaka University. His dedications made my life in Japan much more pleasant and fruitful.

I also want to thank Prof. Tomoo Ushio, who has taken care of me since my very first day in Japan. I am deeply impressed by his extensive knowledge of lightning and meteorology. Discussions with him are always delightful and beneficial.

I am grateful for Prof. Satoru Yoshida, who is always working together with us. He instructed me in making the recording system by USRP, which has been a great experience for me, and the new system will be an essential part for my future research.

I'd also like to thank Prof. Takeshi Morimoto, Prof. Gwan Kim and Prof. Yoshitaka Nakamura for their support and valuable suggestions both on my daily life and my research. Much gratitude is to Prof. Daohong Wang of Gifu University, who gave me valuable suggestions and assistance for me to come to Osaka University and took great care of me during my stay in Japan. Many thanks are to Ms. Yoshiko Nishitashi and Ms. Fumie Imura, various helps from whom have made my life and research much easier.

Student members in Kawasaki lab also gave me many helps. Special thanks are to Mr. Yuji Takayanagi, without whose help many works would be much more difficult to do. Dr. Manabu Akita, Mr. Hiroshi Kikuchi, Mr. Akihiro Sakatani, Mr. Naoya Kitade, among many others, also provided me significant help for my research. I want to thank all the members in Kawasaki lab for being so kind to me, and for the best memory of working and having fun together.

Some parts of this thesis are based on my work in Chinese Academy of Meteorological Sciences (CAMS). I also want to thank professors and student members in CAMS for their contributions.

Financial support for my study in Osaka University is provided by Yoshida Scholarship Foundation. I want to express my gratitude to this great foundation.

Finally, I want to thank my parents and my wife for their support, patience and love.

Contents

Chapter 1

Introduction

1.1 Basic types of lightning discharges

Lightning is an atmospheric electrostatic discharge with very short duration and very high voltage. Lightning is mainly produced in thunderstorms. A typical mature thunderstorm in summer usually has three charge layers: main negative charge layer, upper main positive charge layer and lower positive charge layer. The electric field strength between main negative charge layer and upper positive charge layer is usually the strongest, so discharge breakdowns in this region are most easily to happen. Such discharge is called intracloud lightning (IC) as it is produced inside cloud or sometimes between different clouds without connecting to the ground. A discharge process connecting to the ground is called cloud-to-ground lightning (CG). There are positive CG (+CG) and negative CG (–CG). –CG typically accounts for about 90% of all CGs, transferring negative charges to the ground. +CG is much fewer, usually initiated from the upper positive charge layer, transferring positive charges to the ground.

CGs only account for about 20% of all lightning, but they exert the most serious damages to different kinds of properties and even humans on the ground. Lightning strikes carry an electric current of 30 kA on average. It is a constant threat to power lines. Electronic devices such as telephones and computers are also easily to be damaged by overcurrents produced by lightning. Lightning is also a major reason for forest fires. If a lightning strike is close to a human, it can cause severe injuries or even death. An estimated 24,000 people are killed by lightning strikes around the world each year and about 240,000 are injured.

ICs are much more common than CGs, but they are much less well studied. One major reason is that ICs induce much less hazard to ground-based objects and humans. Another reason is that it is much more difficult to observe and study ICs. For example, discharge channels of ICs are usually blocked by clouds and cannot be observed directly by high-speed video; ICs do not connect to the ground, so it is very difficult to directly measure currents and charge transfers produced by ICs. ICs are mainly produced between the main negative charge layer and the upper positive charge layer. Sometimes they are also found below the main negative charge layer.

Narrow bipolar event (NBE) is also a type of ICs. It is called narrow bipolar event because it produces narrow (< 10 μs) and bipolar electric field change waveform. Normal ICs sometimes also produce narrow and bipolar pulses, but NBE has many other special characteristics, including very strong VHF radiation, temporal isolation, high altitude and short channel length. Because of its short channel length (< 1 km), NBE is also called compact intracloud discharge (CID) by some researchers. There are two polarities of NBEs. Various differences between positive and negative NBEs will be extensively investigated in this thesis.

1.2 Overview of researches on NBE

1.2.1 Discovery of NBE

NBE was first discovered by Le Vine in 1980 when he was trying to find the lightning discharge process producing the strongest VHF radiation [*Le Vine*, 1980]. He found such process produced a bipolar pulse lasting 10 to 20 μs as shown in Figure 1.1. At that time, Le Vine thought this might be a special type of K change process, but he also pointed out some differences compared with K change process.

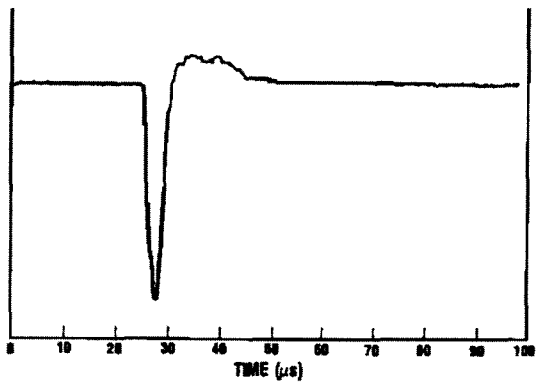

Figure 1.1 Electric field change waveform of NBE recorded for the first time. Adapted from *Le Vine* [1980].

Similar waveforms were observed in Sri Lanka in 1985 by *Cooray and Lundquist* [1985], but they only presented basic features of waveforms without further analysis.

Electric field and field-derivative waveforms produced by NBE were extensively analyzed for the first time by *Willett et al.* [1989]. They found that waveforms produced by NBE were obviously different from those produced by normal lightning discharges. Waveforms produced by NBE have no apparent association with K changes or other discharge processes. They named such discharge event as narrow bipolar pulse (NBP) based on its waveform shape. This study separated NBE from other lightning discharge processes and

treated it as an independent discharge event for the first time.

Smith et al. [1999] systematically studied various features of NBE including pulse width, pulse peak, temporal isolation, discharge height and the relationship with thunderstorm. They also found that NBE is the radiation source of the so-called "TIPPs" (Transionospheric Pulse Pairs) [*Holden et al.,* 1995] observed from satellite. Although this study only analyzed a small sample of NBEs from three thunderstorms and all of the NBEs are positive ones, it established that NBE is a special type of lightning discharge that is distinctly different from other lightning processes. After this study, NBE has drawn wide attention as an independent discharge event.

1.2.2 Observation of NBE from satellite

The first satellite observation of NBE was made by ALEXIS satellite in the 1990s [*Holden et al.,* 1995]. Several hundred unusual radiation signals occurring in pairs were recorded and dubbed as TIPPs. A time-frequency plot of a typical TIPP is shown in Figure 1.2. At that time, no one knows what the source of such signals is. In 1999, *Smith et al.* [1999] found that TIPPs are originated from VHF radiation of NBEs. Now it is well established that NBEs produced extremely energetic VHF radiation which can propagate through the ionosphere and observed by satellite. The signal received by satellite has distinctive features as in Figure 1.2, so it is very convenient to observe NBE from satellite.

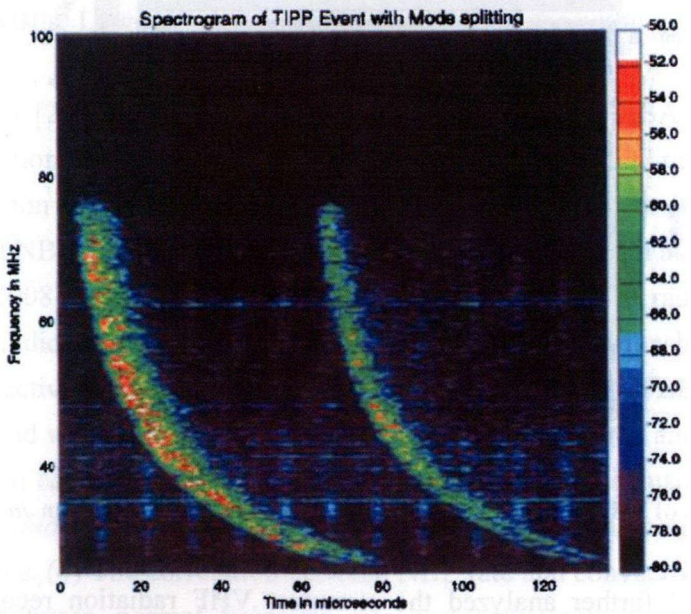

Figure 1.2 Time-frequency plot of a TIPP event, which is the radiation signal of NBE observed by satellite. Adapted from *Holden et al.* [1995].

Light and Jacobson [2002] analyzed VHF radiation and optical emission of NBE recorded by FORTE satellite, and found that VHF radiation of NBE is indeed much more

energetic than that of non-NBE. A surprising result is that NBE is rarely accompanied with optical emission. In another word, NBE is a type of "invisible" lightning.

Jacobson and Light [2003] further analyzed characteristics of VHF radiation recorded by FORTE satellite. They found two different types of characteristic signals as shown in Figure 1.3. The signal in Figure 1.3(a) is much stronger than that in Figure 1.3(b), and they demonstrated that the signal in Figure 1.3(a) is produced by NBE while that in Figure 1.3(b) is produced by normal intracloud lightning. They concluded that VHF radiation of NBE is two to three times higher than that of non-NBE. They also found that NBE is usually temporally isolated with other discharges or appears as the initiation process while non-NBE can occur in any phase of intracloud lightning.

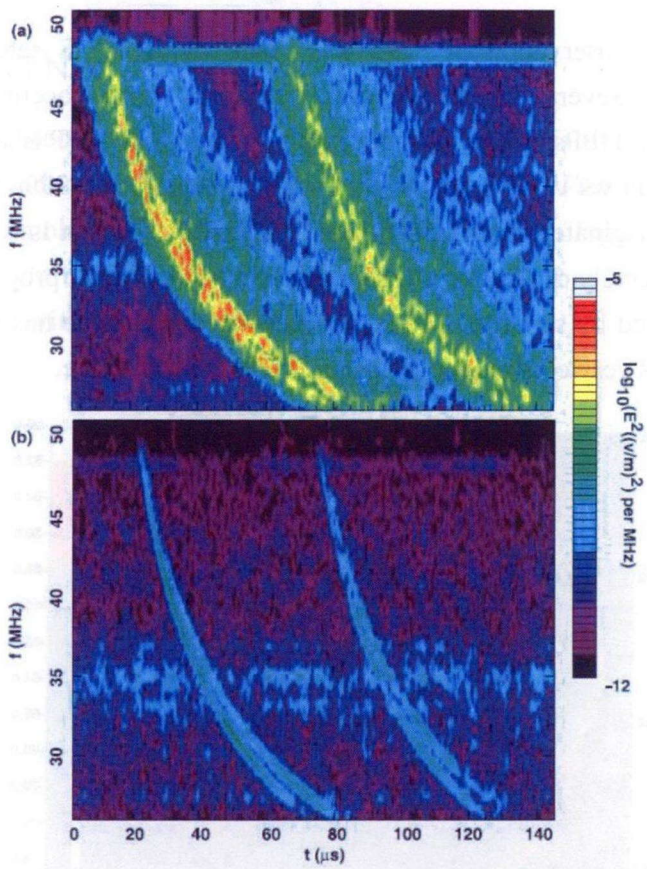

Figure 1.3 Two types of VHF signals recorded by FORTE satellite. Adapted from *Jacobson and Light* [2003].

Jacobson [2003] further analyzed the strongest VHF radiation recorded by FORTE satellite and found that not all of the signals with strong radiation are produced by NBE. Non-NBE sometimes can also produce very strong VHF radiation.

1.2.3 Relationship between NBE and thunderstorm

Since NBE can be conveniently observed by satellite, it is a potential candidate for monitoring convective activities from satellite if NBE has certain relationship with thunderstorm. Therefore, many studies tried to investigate such relationship. Such studies were mainly based on lightning data of Los Alamos Sferic Array (LASA) [*Smith et al.*, 2002], which covers a wide area and can detect different types of lightning discharges.

Suszcynsky and Heavner [2003] used two-year data of LASA and analyzed the relationship between NBE and CG. They treated CG rate as an indicator of convective strength of thunderstorm. The result showed that as CG rate increases, NBE rate also has obvious increasing tendency, but the correlation between NBE rate and CG rate has large variance. They also found that height of NBE has the tendency to increase with increasing rate of NBE. This indicates that NBE rate increases as the thunderstorm develops higher.

Jacobson and Heavner [2005] used three-year data of LASA and made more detailed analysis. They used cloud-top temperature inferred from infrared cloud imagery to indicate the convective strength. Such parameter is a much more direct and accurate indicator of convective strength than CG rate used by *Suszcynsky and Heavner* [2003]. They found that NBE and non-NBE are produced in the same meteorological environment, so they stated that NBE rate can be used to indicate convective strength of thunderstorm as CG and IC. But they also found some differences between NBE and normal lightning discharges. For example, one thunderstorm only produces single polarity of NBE. NBEs are more temporally and spatially compact than non-NBEs. Large numbers of NBEs tend to cluster within a short period and in a small area.

Lapp and Saylor [2007] used two-month data of the upgraded LASA [*Shao et al.*, 2006] and analyzed correlation between NBE, CG and IC. They found that CG rate and IC rate have quite strong correlation while the correlation between NBE and CG or IC is much weaker. They concluded that NBE cannot be used to indicate convective strength as CG or IC.

Wiens et al. [2008] made the most detailed analysis. They used radar reflectivity and 30-dBZ height to indicate convective strength, and analyzed relationship between NBE, non-NBE and convective strength. Their major conclusions are: (1) NBEs are much fewer than CGs and ICs, and when they occur, they tend to be in a small area and in a short period. (2) One thunderstorm can produce both polarities of NBEs. This conclusion is contradictory to that of *Jacobson and Heavner* [2005]. (3) When NBE occurs, the convective strength is usually more vigorous. (4) The correlation between NBE rate and convective strength is much weaker than that between normal lightning rate and convective strength. At last, they concluded that NBEs are usually associated with very vigorous convection, but even the most vigorous thunderstorm may not produce NBE. This is probably the most convincing conclusion so far as for the relationship between NBE and thunderstorm. It means NBE is produced in very vigorous thunderstorm, but some conditions other than strong convection

are required for the production of NBE.

1.2.4 Estimation of NBE discharge parameters

For any type of lightning discharge, it is very important to know various discharge parameters such as current magnitude, current velocity and transferred charge. There are many studies to estimate these parameters for NBE.

Smith et al. [1999] first roughly estimated dipole moment changes of NBE from fast electric field waveforms. The average dipole moment change for 15 NBEs was 0.38 C·km. They also estimated that the channel length of NBE was no more than 1 km.

Eack [2004] recorded NBE electric field change waveforms at both close and far distances. On the basis of such records, he calculated that the average charge transferred during one NBE is 0.3 C, channel length is 3.2 km and travelling velocity of current is 1/3 of light speed. However, *Nag and Rakov* [2010a] stated that such a calculation has some errors and the channel length of 3.2 km is an overestimation.

Hamlin et al. [2007] found that for some NBEs, there is a small pulse after the main pulse of NBE. As shown in Figure 1.4, they suggested that the pulse β was produced by reflected current in the channel. Based on such mechanism, they calculated channel length of NBE from the time difference between pulse α and β (Δt). Under the assumption of current velocity equaling light speed, they got the upper limit of channel length of NBE as 2 km.

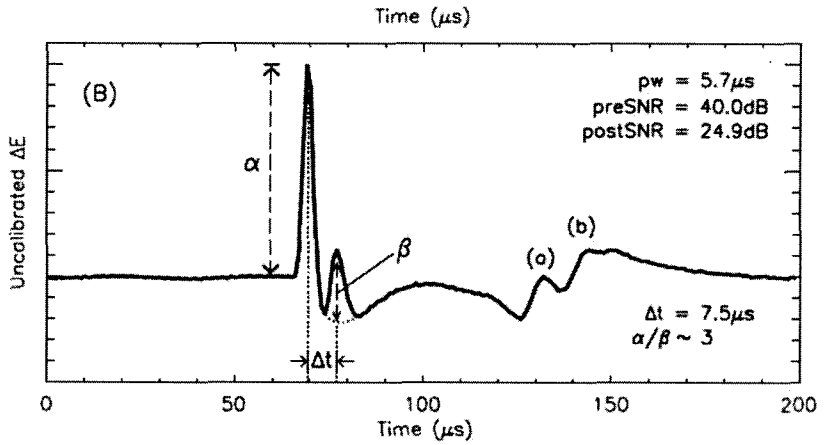

Figure 1.4 Electric field change waveform of NBE with secondary pulse caused by current reflection. Adapted from *Hamlin et al.* [2007].

Watson and Marshall [2007] used a modified transmission line model to fit the close-field and far-field waveforms of NBE presented by *Eack* [2004]. When they set the current as exponentially increasing and negative charge moving upward, their model result agreed with the observation of *Eack* [2004]. Based on the modeling result, they estimated a charge moment of 0.6 C·km, current velocity of 6×10^7m/s and channel length of 630 m.

Nag and Rakov [2010a, 2010b] analyzed dE/dt waveforms produced by NBE and

suggested that current was reflected in NBE channel for multiple times within several microseconds. Based on such observation, they proposed a current oscillation model and estimated the current velocity between 0.3×10^8 to 3×10^8 m/s. Further they used Hertzian dipole approximation to calculate discharge parameters of NBE. Their results are current peak of 143 kA, current rise time of 5.4 μs, charge transferred within the initial 5μs of 303 mC.

Liu et al. [2012] made the first observation of NBE channel with digital interferometers. They found that the vertical scale of NBE channel is from 0.4 to 1.9 km and the current velocity is from 0.56×10^8 to 2.6×10^8 m/s.

1.3 General characteristics of NBE

On the basis of the findings reported by previous studies, here I summarize the general characteristics of NBE.

(1) NBE emits the most powerful radiation in VHF radio frequency, which is usually several times larger than other lightning processes. Such signal can propagate through the ionosphere and be observed by satellite.

(2) NBE produces narrow and bipolar electric field change waveform in VLF and LF radio bands. This is also why it is called "narrow bipolar event". Figure 1.5 shows waveforms of typical +NBE, –NBE and –RS. Waveforms of NBEs are obviously different from that of return strokes, so in many studies NBEs are automatically identified by their VLF and LF electric field change waveforms. This thesis is also mainly based on such waveforms.

(3) Lightning discharge channels can be recorded by videos and cameras, and we can study the channel characteristics with these recordings. For NBEs, however, there is so far no such observation. Studies based on satellite observation suggest that NBE produces relatively weak radiation in visible spectrum.

(4) A complete lightning discharge usually comprises many processes. For example, a cloud-to-ground lightning at least comprises preliminary breakdown, followed with stepped leader and return stroke. However, NBE is usually found isolated with other discharge processes. Sometimes it is also found to be the initiation of otherwise normal lightning.

(5) The channel length of normal lightning is usually several kilometers long, sometimes as long as 20 km. However, the channel length of NBE is inferred to be less than 1 km.

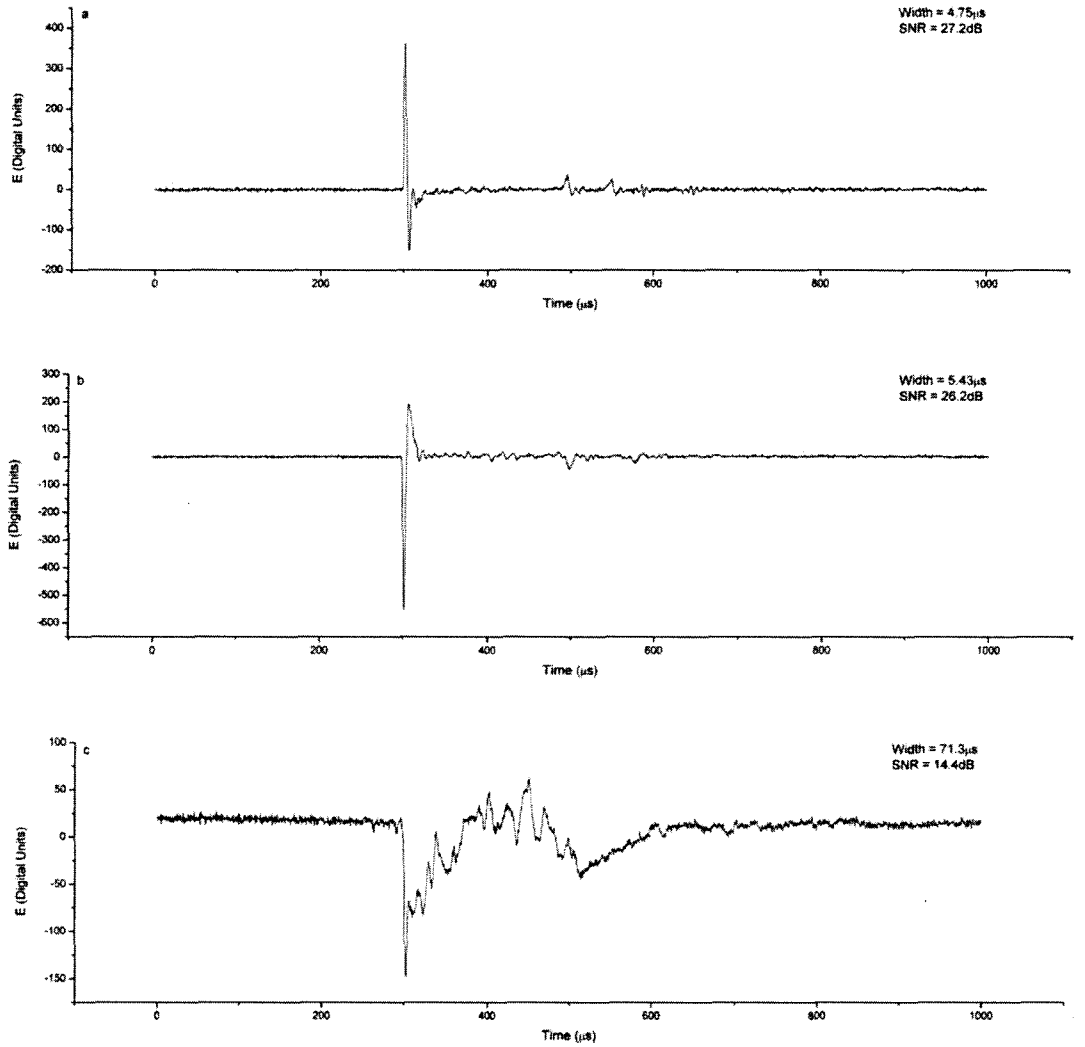

Figure 1.5 Typical waveforms of (a) +NBE, (b) –NBE and (c) –RS.

1.4 Objective and overview of this thesis

This study will try to solve one of the most important questions on NBE: is it possible to use NBE to monitor severe thunderstorm? There have been many studies on this issue, but most of them are statistical study and the results are not consistent with each other. In our study, we have recorded large number of NBEs in different regions, and based on the observation of phased array radar (PAR), we can correlate NBE production with detailed structure of thunderstorm. Different characteristics of NBE in different regions will also reveal certain clues as to the production mechanism of NBE in thunderstorms.

In Chapter 3, I will first analyze the waveform characteristics of NBE, which is essential for NBE classification. I will also discuss the temporal isolation of NBE, which is important

for understanding relation between NBE and normal lightning.

In Chapter 4, I will analyze the discharge height of NBE. Discharge height of NBE plays a crucial role in associating NBE and thunderstorm because it determines NBE position relative to a thunderstorm, which further determines meteorological context of NBE production. I will develop a new method for locating NBE using ionospheric reflection of NBE signal. This method is much more accurate for determining NBE height than traditional TOA technique. With this method, I will calculate discharge height of thousands of NBEs and analyze the height distribution. I will also show variation of NBE height during two thunderstorms.

In Chapter 5, I will first analyze the statistical relation between NBE and thunderstorm similar with previous studies. Then I will analyze some cases based on the observation of PAR. PAR observation shows some characteristic feature on the spatial relationship between NBE and thundercloud, based on which I will propose a way to monitor severe thunderstorm with NBE.

Some important issues will be discussed in Chapter 6 and conclusions will be drawn in Chapter 7.

Chapter 2

Experiment, instrumentation and data

2.1 Experiment

This thesis is based on four experiments, two in China and two in Japan. The time, location and equipment are summarized in Table 2.1 and are described below.

Table 2.1 Summary of four experiments for this thesis

Period	Location	Equipment	Note
Aug. 6 ~ Aug. 24, 2007	Guangzhou, China	LF lightning location system; C-band radar	
Jun. 27 ~ Aug. 23, 2010	Chongqing, China	LF lightning location system; C-band radar	
Dec. 2010 ~ Jan. 2011	Hokuriku, Japan	LF lightning location system	For observing winter thunderstorm
Jul. 6 ~ Sep. 14, 2012	Osaka, Japan	LF lightning location system; PAR	

2.1.1 Observation in 2007 in Guangzhou, China

In the summer of 2007, an LF lightning locating network consisting of 7 stations of fast electric field change meters were established in Guangzhou, China. All the electric field change meters were identical to each other and were similar in principle to that described by *Kitagawa and Brook* [1960]. The electric field change systems had a decay time constant of 1 ms. The output was digitized at 10 MHz with a resolution of 12 bits and each record had duration of 1 ms. Each recorded event was time stamped with GPS receivers, and three-dimensional position of the sources can be determined employing TOA technique.

As shown in Figure 2.1, five of the stations were located around the central station with a distance of about 10 km, and another station was located about 32 km away from the central station. Such a compact configuration is largely different from that of other lightning locating systems such as LASA [*Shao et al.,* 2006], which has baselines of larger than 100 km. The reason that we closely located these stations was to carefully and thoroughly study those storms passing over the stations, in the way of making total-lightning observations. There is

also an obvious limitation, though, that the location accuracy is relatively low for the discharges far away.

Because this is the first experiment, many techniques were not mature enough. We started to build this system since May, 2007, and this system started to work stably since August. Data from Aug. 6 to Aug. 24 are used for this thesis.

A C-band weather radar near the system was used to observe reflectivity of thunderstorms.

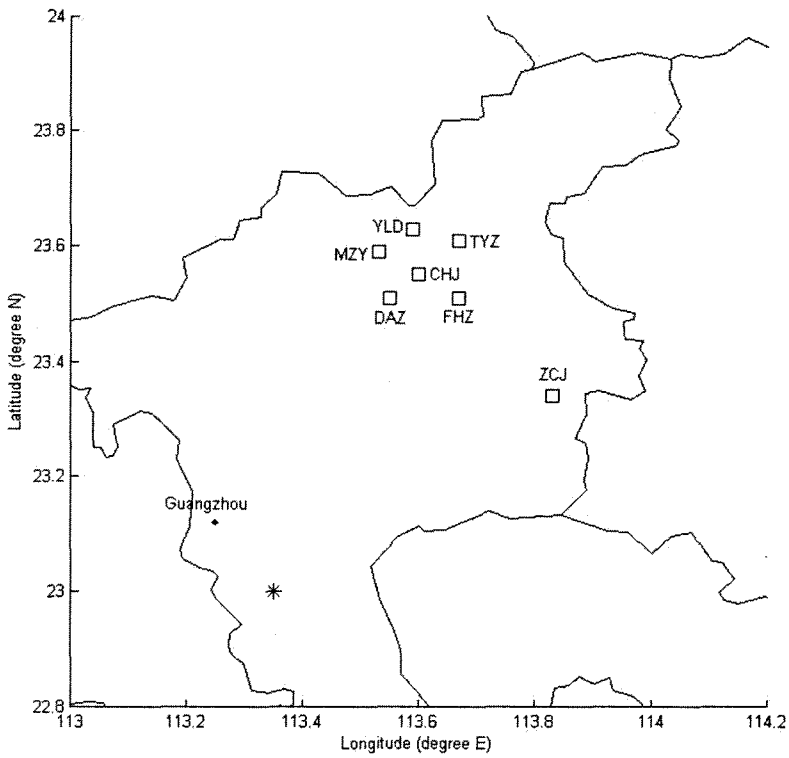

Figure 2.1 Locations of LF lightning location system and C-band radar for observation in Guangzhou, China. Observation stations are represented by squares and radar is represented by "*".

2.1.2 Observation in 2010 in Chongqing, China

A similar LF lightning location system comprising nine stations were established in Chongqing, China in the summer of 2010, as shown in Figure 2.2. This system covered an area with a radius of about 30 km, much larger than the one in Guangzhou, China. This system had continuously worked from May to October, 2010. Data from Jun, 27 to Aug. 23 are used for this thesis.

There was also a C-band weather radar near the system.

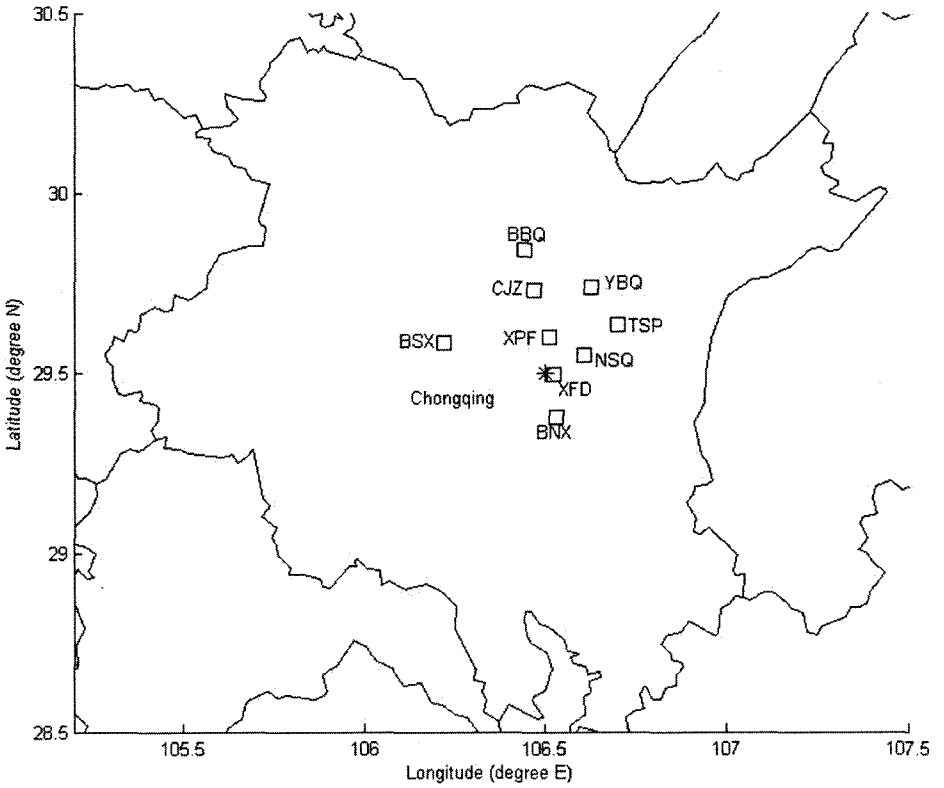

Figure 2.2 As Figure 2.1, but for the observation in Chongqing, China.

2.1.3 Winter observation during 2010-2012 in Hokuriku, Japan

During the winter of 2010-2011, a small LF lightning location system comprising 4 stations was set up in Hokuriku region near the Japan Sea coast as shown in Figure 2.3. Distances between observation stations were about 5 km. Each station was equipped with a fast antenna with a decay time constant of 200 us and frequency range of 400 Hz to 1 MHz. Electric field change signals produced by lightning discharges were recorded by an A/D converter with 4 MHz sampling rate in 12-bit resolution. 3-D locations of lightning discharge events observed simultaneously by 4 stations were determined by interferometry technique. Details of this system were described by *Takayanagi et al.* [2011].

Because this system covers a quite small area, it could only accurately locate discharge events close with this network. Therefore, we use the information of lightning location system (LLS) in Japan to get the location of return strokes. LLS in Japan is operated by electric companies of Japan and has a location accuracy of about 0.5 km [*Matsui and Takano,* 2010].

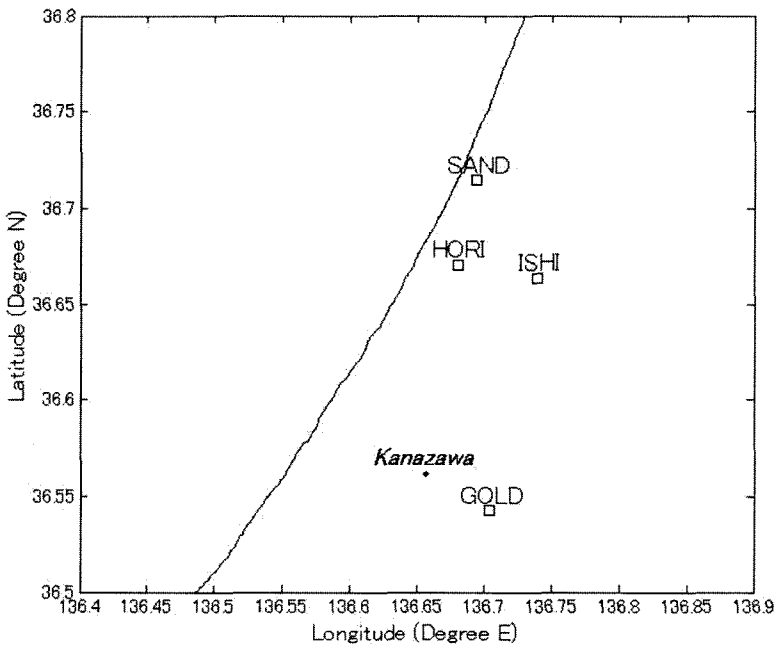

Figure 2.3 As in Figure 2.1, but for observation in Hokuriku, Japan.

2.1.4 Observation in 2012 in Kansai, Japan

LF lightning location system in Osaka region of Japan has been set up since the summer of 2011. During the summer of 2012, there were 9 stations as shown in Figure 2.4. This system covers an area with a radius of about 40 km, and the site NGHL has a long baseline of about 100 km, enabling accurate location of lightning discharges in a large area. The frequency range and sampling rate of this system are the same as the one in Hokuriku.

The PAR was installed in Suita campus, Osaka University. It started working since July 6, 2012. It has very high temporal and spatial resolution, enabling us to observe detailed structure of rapidly evolving thunderstorms. Details of PAR will be described in section 2.2.2.

Since the PAR started working on July 6, lightning data from the same day are analyzed. And because there were few thunderstorms since October, 2012, I have only analyzed data before September 14.

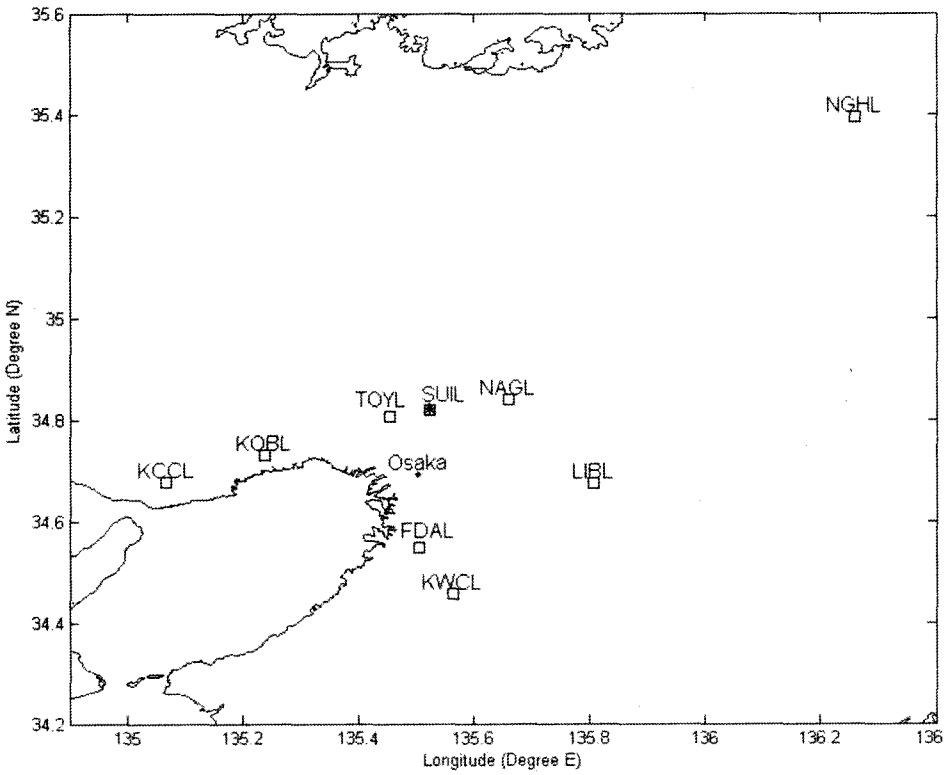

Figure 2.4 Locations of LF lightning location system and PAR in Osaka, Japan. Observation stations are represented by squares, and the PAR is represented by "*".

2.2 Instrumentation

2.2.1 LF lightning location system based on USRP

In each experiment, we had an LF lightning location system. These systems have quite similar components and functions. Here I only introduce our newest version based on USRP (Universal Software Radio Peripheral).

Generally speaking, USRP is a type of software radio. The USRP is connected with a host computer through a Gigabit Ethernet link, and the host computer can control the USRP and do the data transmission and receiving. All the waveform-specific processing such as modulation and demodulation are also done on the host computer. One USRP is usually consisted of three parts: motherboard, daughterboard and GPS disciplined oscillator (GPSDO). The motherboard provides basic components required for signal processing including FPGA, ADCs, DACs and power regulation. There are several types of daughterboards for different

purposes. We are using a LFRX daughterboard which works as a receiver in DC to 30 MHz radio bands. The GPSDO is a combination of a GPS receiver and a high-quality, stable oscillator. It can provide a time reference accurate to nanoseconds.

A crucial advantage of USRP is that it can digitize signal into memory while at the same time writing records to hard disk. In such a way, it has absolutely no dead time. Dead time was a common problem for lightning recording systems. When lightning discharge triggers the system, the system needs to stop to write the stream onto hard disk, and the signal during the period of writing is lost. The USRP has perfectly solved this problem. A comparison between USRP and old systems is shown in Figure 2.5. It shows one-second waveforms recorded by different stations. The first station was using USRP while the others were using old system. During that period, lightning discharges were very frequent. The waveform in the first panel shows continuous triggering. This station recorded all of the signals in this period. For the old systems, there was always some dead time between two triggers. During the dead time, the signal was not recorded and was lost.

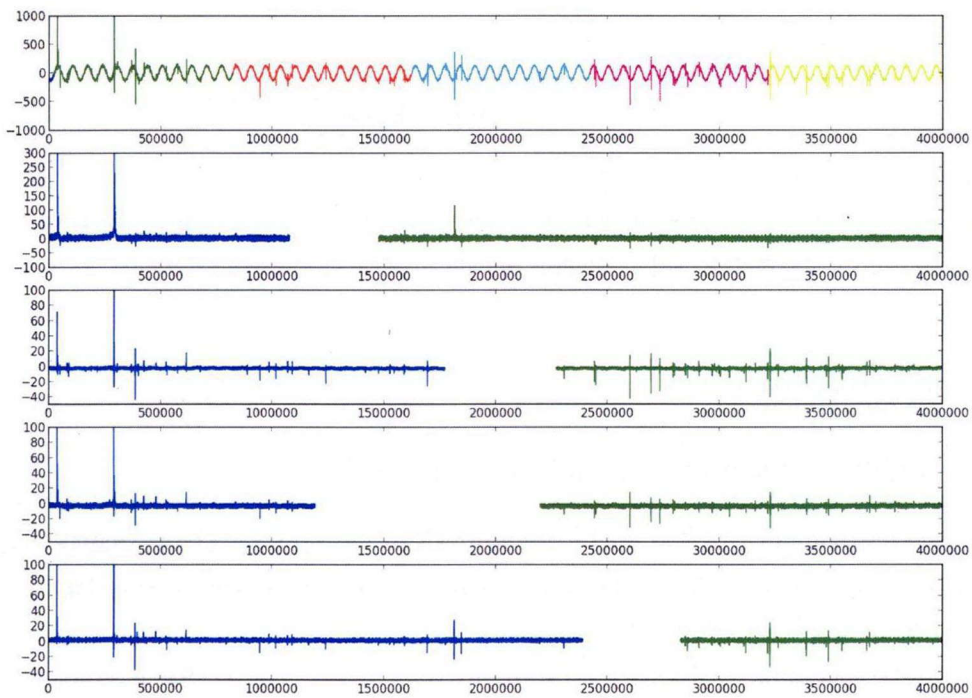

Figure 2.5 One-second waveform recorded by different stations of LF lightning location system. The first panel was recorded by a station using USRP. Others were recorded by old A/D converters.

The main components of a single station are a flat plate antenna, A/D converter (USRP) and a computer as shown in Figure 2.6. The flat plate antenna detects electric field change

signals produced by lightning discharges. The USRP receives and digitizes the signal and transmits it to the memory of the computer. The computer processes the digitized signal and writes a designated length of signal onto hard disk when the signal triggers the system.

Figure 2.6 Main components of a single station of LF lightning location system.

Figure 2.7 shows the configuration of LF lightning location system. The parts inside the red square constitute a single station. Each station has a part outside room and another part inside room. Based on different conditions, the part inside room is sometimes put inside a box and installed outside. Time-stamped data of each station are transmitted back to the server. The server collects data from different stations and calculates 3-D locations of lightning discharges.

2.2.2 Phased array radar

The PAR started working since July, 2012. It is a single-faced phased-array system located in Suita campus, Osaka University. In our system, the beam is electronically steered in elevation direction by transmitting a fan beam and receiving scattered signals as multi-beam using digital beam forming technology [*Yoshikawa et al.,* 2012]. In this way, one rotation of the antenna can cover a whole volumetric scan, and the time for volumetric updates can be significantly reduced. The difference between conventional parabolic weather radar and the PAR is illustrated in Figure 2.8. The current system can work in two scanning modes: fast-observation mode and wide-observation mode. Currently the PAR is operated under the wide-observation mode, which takes 30 seconds for a whole volumetric scan and the largest scanning range is 60 km. Its temporal resolution of 30 seconds is far better than conventional weather radar with parabolic antenna. Its spatial resolution is 100 m in radial direction, 1.2° in azimuthal direction and 0.9° in elevation direction. Such spatial resolution is also much better

than conventional weather radar.

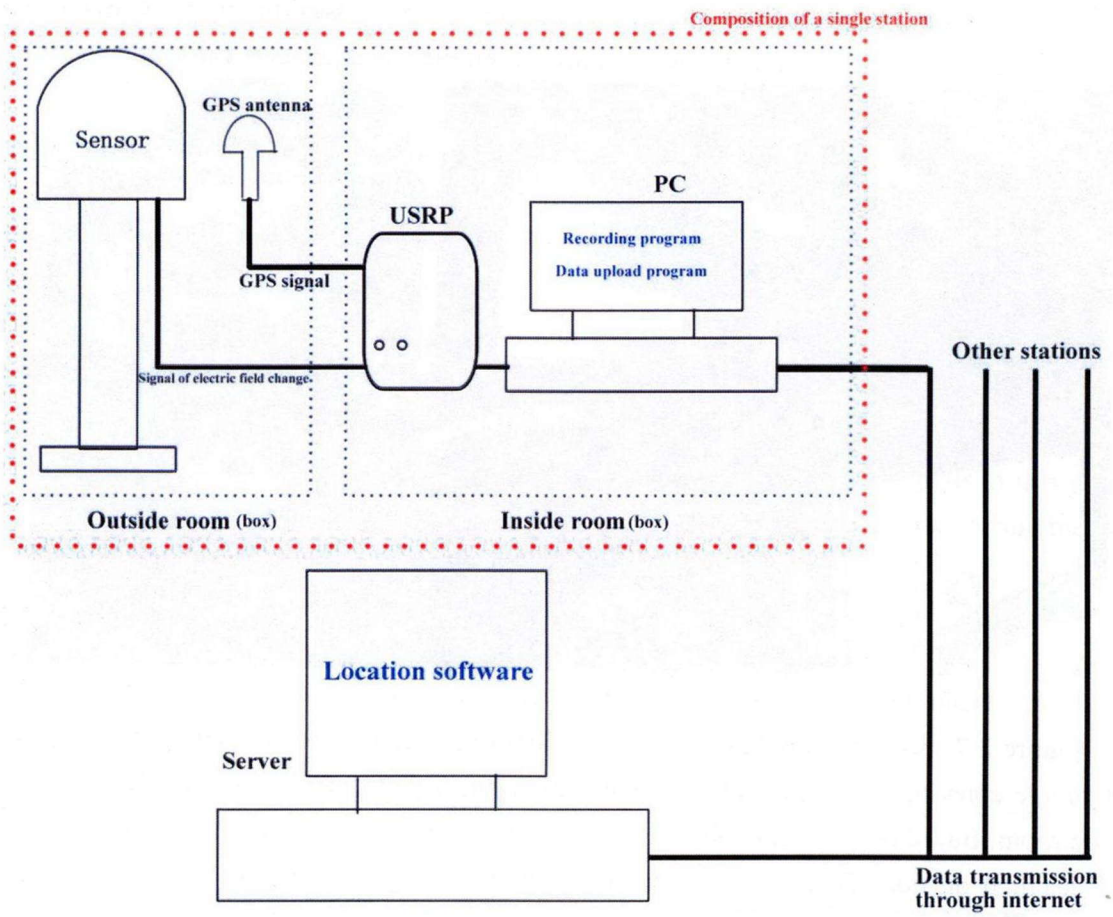

Figure 2.7 Configuration of LF lightning location system.

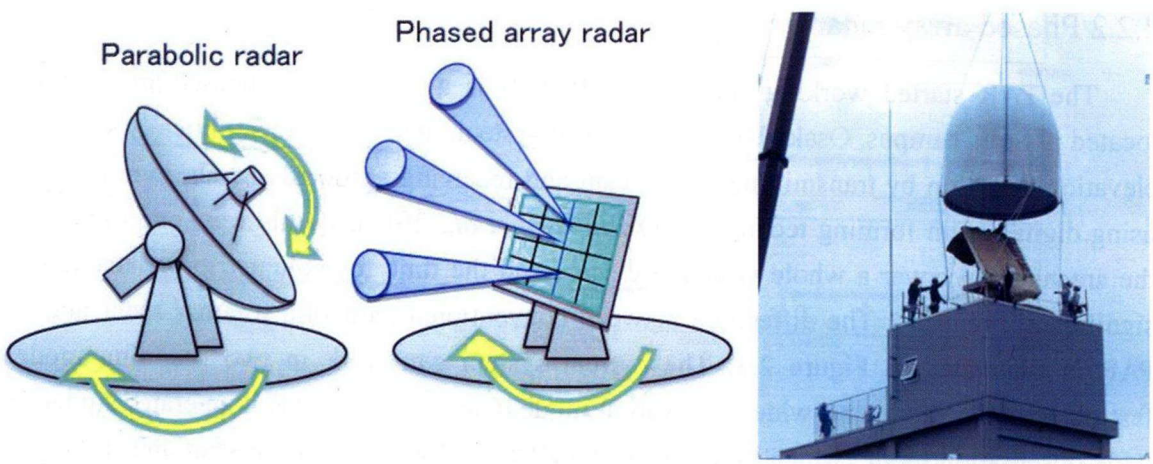

Figure 2.8 Illustration of difference between conventional parabolic weather radar and phased array radar.

Data quality has not been fully controlled. The reflectivity data commonly contain some contaminations from ground clutters, such as the dark blue region in lower part of Figure 2.9. Echoes from such contamination have strong intensity (larger than 50 dBZ), but they only occur at a low altitude (lower than 2 km). Therefore I use height of 20 dBZ to indicate evolution of thunderstorms as shown in Figure 2.9. Another problem is that observation within about 10 km of the PAR is not very accurate due to some unsolved problems on pulse compression in this newly-build system. So data within 10 km of the PAR are not shown.

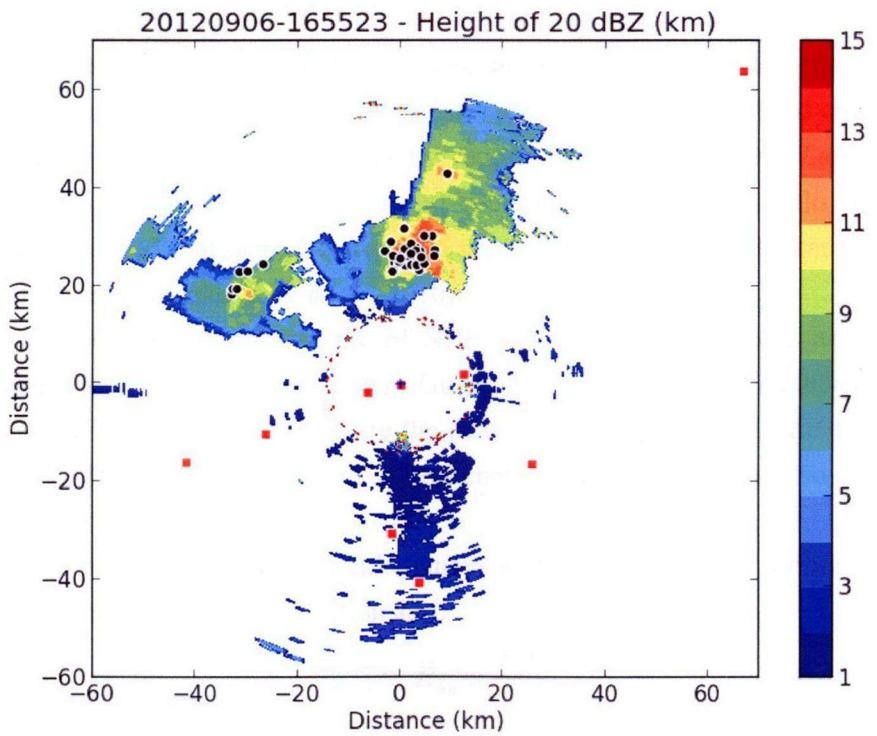

Figure 2.9 Height of 20 dBZ calculated from PAR reflectivity data. The PAR is represented by blue "+". Nine stations of LF lightning location system are represented by red squares. Black points represent lightning locations within ±15 seconds of the radar time.

2.3 Summary of data

Data of different types of lightning discharges recorded in each experiment are summarized in Table 2.2. In the experiments in Guangzhou and Chongqing, number of +RS was not counted because +RS was relatively rare in those regions and was not analyzed. In the experiment in Hokuriku, no NBE was recorded, but a special type of discharge named isolated large bipolar pulse (ILBP) was recorded. ILBP will be analyzed in section 6.1. In the

experiment in Osaka, only NBEs were analyzed.

Table 2.2 Summary of number of different types of lightning discharges in each experiment.

	+RS	–RS	+NBE	–NBE	other
Guangzhou	×	138148	7882	3994	
Chongqing	×	174756	36442	7893	
Hokuriku	36	131	0	0	ILBP 14
Osaka	×	×	232	22	

* × means not counted

Chapter 3

Waveform characteristics of NBE

3.1 Pulse peak magnitude

It has been noticed that NBE produces quite large electric field changes since its first discovery. *Le Vine* [1980] reported that peak magnitude of electric field change produced by NBE was about 1/3 of that produced by return stroke. *Cooray and Lundquist* [1985] had similar observation. *Willett et al.* [1989] reported an even high ratio of 0.72. A recent observation showed that peak electric field change produced by NBE can be larger than that produced by return stroke [*Nag et al.*, 2010].

In previous studies, the sample of NBE was usually quite small, and only +NBE was considered. Here I will use the data in Guangzhou, China, which includes large number of +NBEs, –NBEs and –RSs, to compare the peak magnitude of electric field changes produced by NBE and RS. The value of electric field change was not calibrated, so digital unit (DU) is used.

In order to compare electric field changes at different distances, I normalize electric field to 100 km using the following relationship:

$$E_{nor} = \frac{E \cdot R}{100} \tag{3.1}$$

where E is recorded electric field change, R is the distance between the discharge event and the observation station in kilometers, and E_{nor} is the electric field normalized to 100 km.

Because the relationship in (3.1) is only valid for radiation field, and electric field produced by lightning discharges more than 50 km away can be treated as only containing radiation field component, here I only analyze discharge events farther than 50 km from observation station.

The mean values of electric field changes normalized to 100 km are 430, 685 and 243 DU, respectively, for +NBEs, –NBEs and –RSs. It seems both +NBE and –NBE produced larger electric field changes than –RS does, and –NBE is even stronger than +NBE.

In order to analyze the distribution of electric field changes, the value of 0 - 3000 DU is divided into 60 segments with each segment spanning a value of 50 DU, and the value of larger than 3000 DU is set as another segment, thus totally 61 segments. Then the percentage

of events that fall in each segment is calculated for +NBE, –NBE and –RS, respectively. The result is shown in Figure 3.1. The distribution of –RS is largely different from that of +NBE and –NBE, showing a predominant portion of –RSs having values below 500 DU. The normalized mean value of –RSs is 243 DU, which is 0.56 of that of +NBEs and 0.35 of that of –NBEs. It seems that NBEs are generally more energetic than –RSs in VLF/LF bands. This result is in accordance with a recent study on +NBEs [*Nag et al.*, 2010].

Ratio of normalized mean value of +NBE to –NBE is 0.63. Their distributions of peak values have the same trend (Figure 3.1); the difference is in that a considerably higher percentage of –NBEs than +NBEs have large peak values of electric field changes. For example, there are 34.65% of –NBEs having peak values larger than 800 DU, compared with a value of 11.91% for +NBEs. Besides, there are 14 –NBEs with peak values larger than 3000 DU, while the maximum peak value of +NBE is only 2900 DU. Therefore, –NBEs show a much higher possibility to produce very large electric field changes.

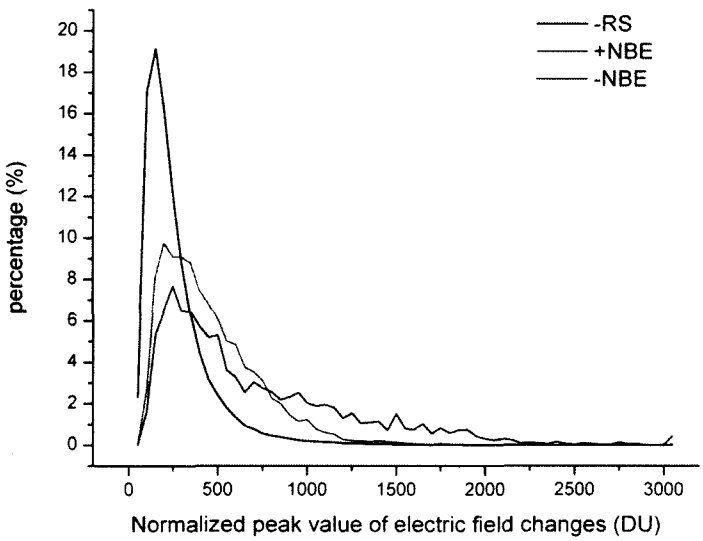

Figure 3.1 Distributions of normalized peak value of electric field changes of –RSs, +NBEs and –NBEs. Each percentage is calculated by dividing the total number of events of each type by the number of events of this type that fall in each 50 DU-long segment.

3.2 Temporal isolation

Le Vine [1980] and *Willett et al.* [1989] both noticed that NBE was rarely associated with other discharge processes. It has been thought that NBE is temporally isolated within tens of milliseconds or even one second. However, more recent observations indicate that at least a significant portion of NBEs serve as the initiation process of normal lightning [*Rison et al.*,

1999; *Betz et al.,* 2008]. *Nag et al.* [2010] also reported several +NBEs that occurred during or after CGs. However, it is still unclear to what extend are NBEs isolated with other discharge processes. In this study, on the basis of large samples of both +NBEs and –NBEs, we try to present some statistical results concerning the characteristic of temporal isolation of +NBEs and –NBEs.

Here I also use the data of Guangzhou, China. Since each record of waveform in this study is 1 ms long, and other discharge signals are rarely observed in the same record with an NBE, I simply define the time difference between two discharge processes as the difference of trigger times of the two records. Considering the possibility that two or more independent discharge processes occur simultaneously at different places, I only consider records of waveforms that are located within 20 km from each other to compute the time difference. Besides, the detection efficiency is relatively low for discharges far away and it is possible to detect NBEs while miss other discharges. In order to limit such detection bias, only those discharges located less than 100 km from the central station are considered. There are a total of 3205 +NBEs and 1969 –NBEs in this area.

11.70% of +NBEs are found to be followed by other discharge processes within 10 ms (defined as post-no-isolation percentage), and 1.59% of +NBEs occur within 10 ms after other discharge processes (defined as pre-no-isolation percentage). The corresponding percentages for –NBEs are 4.42% and 1.73%. It is difficult to tell the distinguishing features merely from these values, but when comparing with the corresponding values of normal discharge processes, the significance of the results is obvious. There are totally 244989 triggering events in the analysis area, and normal discharge processes are picked out simply by excluding NBE records from these triggering events. It is found that the post-no-isolation percentage of normal discharge processes is 12.97%, and the pre-no-isolation percentage is 13.13%. Table 3.1 summarizes these results.

Table 3.1 Characteristics of temporal isolation

	Post-no-isolation percentage	Pre-no-isolation percentage
+NBE	11.70%	1.59%
–NBE	4.42%	1.73%
Normal discharge process	12.97%	13.13%

The above result has twofold meaning. First, it is natural that the post- and pre-no-isolation percentages of normal discharge processes are almost the same. However, by comparison, the post-no-isolation percentages of both polarities of NBEs are much larger than their pre-no-isolation percentages. It indicates that both polarities of NBEs have much higher chance to serve as the initiation processes than to be initiated by other discharge processes. It agrees with the fact that previous studies [e.g., *Rison et al.,* 1999] have observed that NBEs

initiate intracloud discharges while no study has reported any reliable observation of NBEs following other discharge processes on a timescale of several milliseconds. Second, the post-no-isolation percentage of +NBEs, which is close to that of normal discharge processes, indicates that a significant portion of +NBEs are indeed followed by other discharge processes. Such example is not difficult to find in our dataset. Figure 3.2 shows an example of a +NBE followed by typical intracloud discharges. The post-no-isolation percentage of –NBEs is much smaller, indicating that –NBEs are more likely to be temporally isolated with other discharge processes. This is also consistent with the observation by *Rison et al.* [1999] that all NBEs initiating normal intracloud discharges are positive polarity.

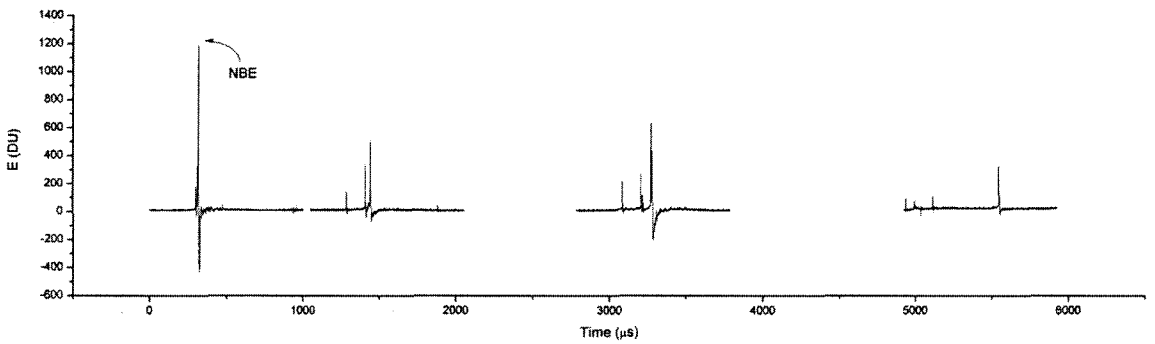

Figure 3.2 An NBE followed by typical intracloud discharges. The distance between two successive discharge events calculated from their locations provided by the LF lightning location system is no larger than 3.5 km, which indicates that these discharges probably belong to the same process.

In some rare cases, NBE is found followed by other discharge processes within one millisecond. Figure 3.3 shows an NBE followed by a –RS within about 0.5 ms. But such case is not common, and there is no evidence that there discharge processes are physically associated, so I will not further discuss it here.

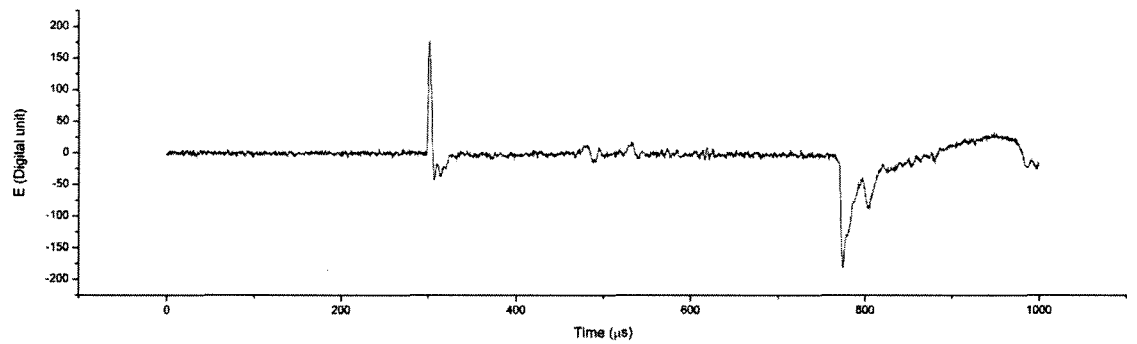

Figure 3.3 An NBE followed by a –RS within about 0.5 ms.

3.3 Ionospheric reflection pairs of NBE

Low frequency radiation of NBE can be reflected between the ground and the D layer of the ionosphere. Although some part of the energy is lost during transmission and reflection, it can still be treated as specular reflection as illustrated in Figure 3.4. Figure 3.5 shows waveforms of NBEs in different distances with ionospheric reflection pairs. As in Figure 3.5(a), the pulse 0 is the direct signal from NBE. When the signal is first reflected by the ionosphere and then received by the station, it forms the pulse 1a. If the signal is first reflected by the ground and then by the ionospheric and then received by the station, it forms the pulse 1b. In Figure 3.5(b), there are two reflection pairs. The second pair is formed when the signal is reflected between the ionosphere and the ground for two turns. The farther the NBE is, the more turns of the reflection are, as shown in Figure 3.5(c) and (d).

One feature in Figure 3.5 is that as the distance between NBE and observation station increases, the magnitude of the first-hop reflection (pulses 1a and 1b) relative to the direct signal (pulse 0) increases. In Figure 3.5(a), the reflection pulses are very small at a distance of less than 200 km. In Figure 3.5(b), the reflection pulses become comparable to the direct pulse. And in Figure 3.5(c) and (d), the reflection pulses are even larger than the direct pulse.

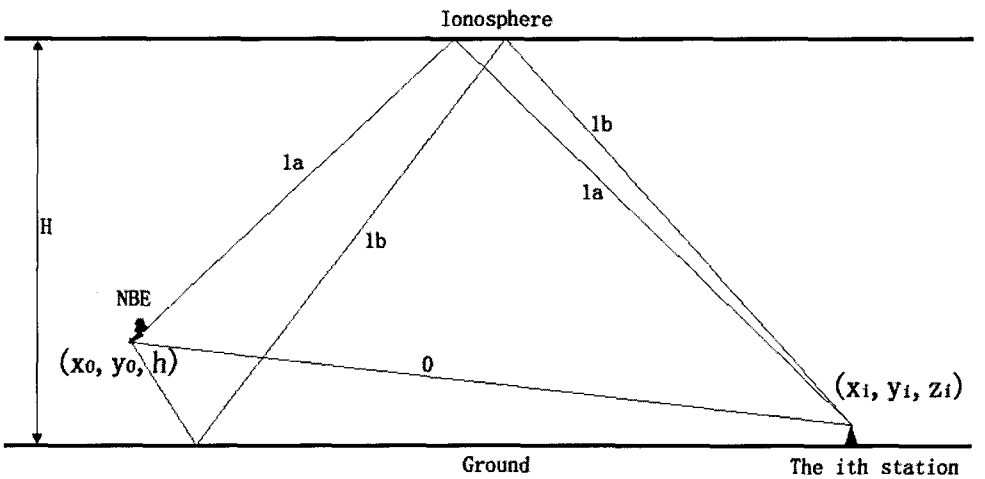

Figure 3.4 Illustration of ionospheric reflection of radiation signals of NBE.

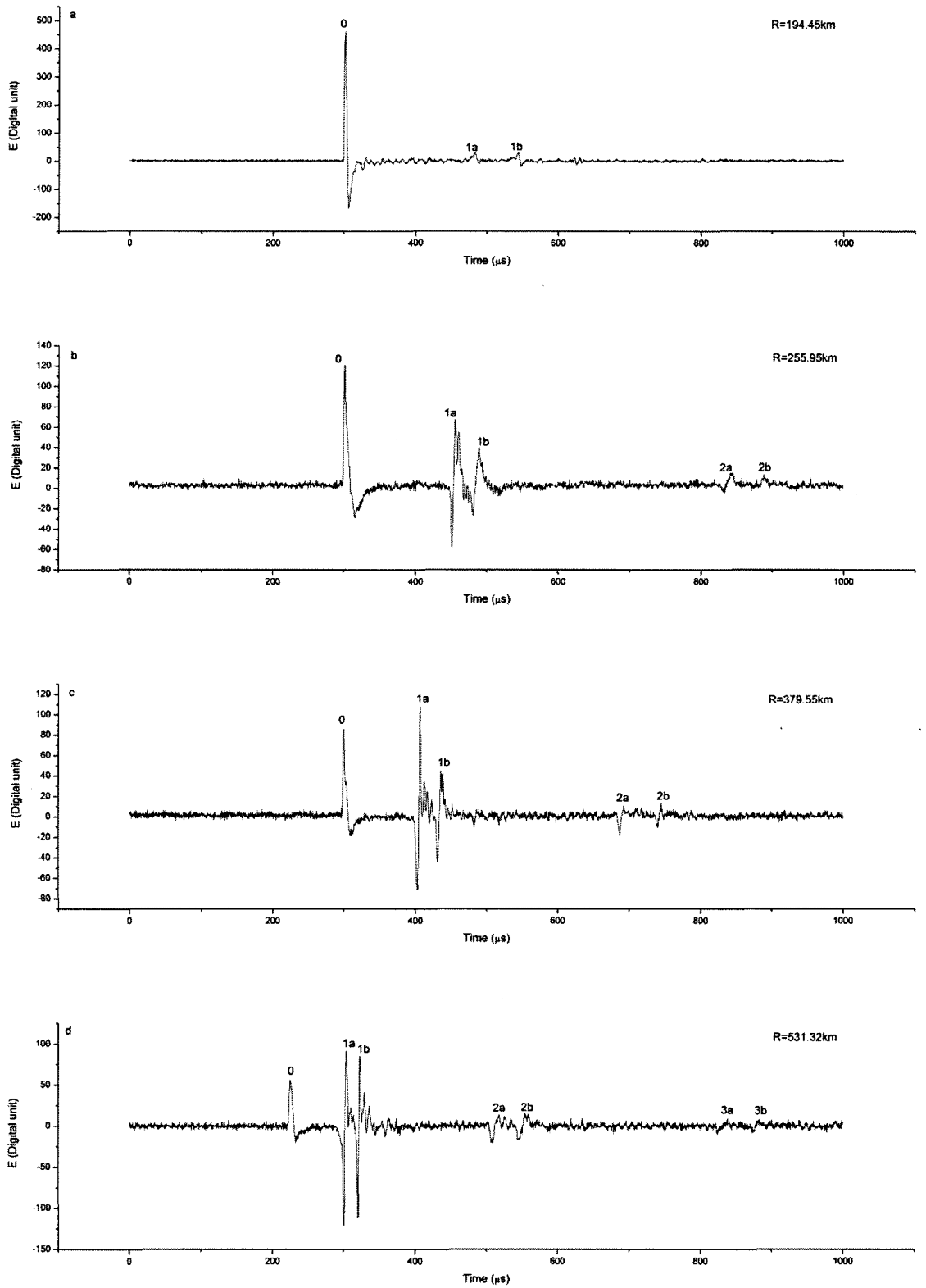

Figure 3.5 Electric field waveforms of NBEs in different distances with ionospheric reflection pairs.

Set the amplitude of direct signal as A_0, the average amplitude of the first-hop reflection pulses as A_1, so their ratio r is:

$$r = \frac{A_0}{A_1} \tag{3.2}$$

And I calculate the value of r for every NBE with ionospheric reflection in Chongqing, China. The result is shown in Figure 3.6. It shows as the distance increases, the ratio r generally decreases. This is because as the distance increases, the incidence angle of reflection increases and more energy is reflected back. On the other hand, the energy of the direct signal decreases due to increasing distance. As a result, the ratio between the direct signal and reflection signals decreases. We can also see that only NBEs farther than about 65 km can produce reflection signals. When NBE is too close with the observation station, the incidence angle of reflection is too small and most of the energy is transmitted through the ionosphere.

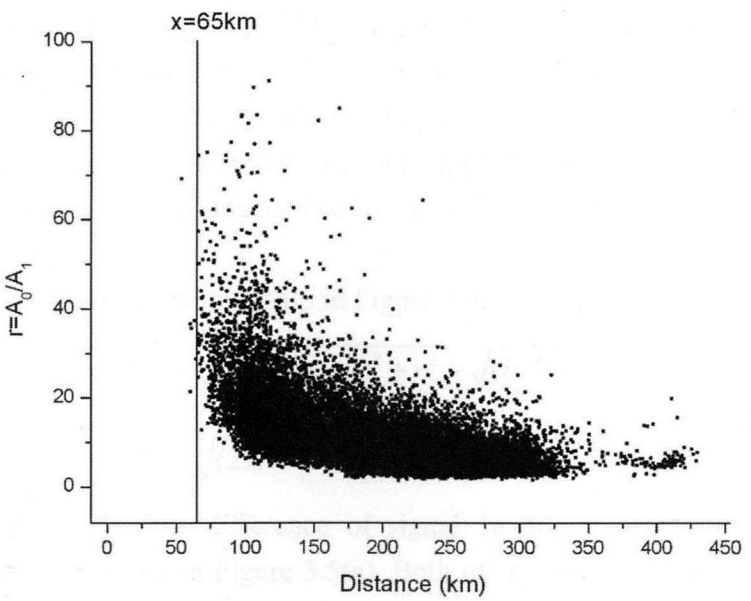

Figure 3.6 Scatterplot of the value r and the distance between the NBE and the observation station for each NBE (Every NBE is observed by multiple stations, so each point represents the observation of one station. The definition of r is in equation 3.2.).

Another feature in Figure 3.5 is that as the distance increases, the time between direct pulse (0) and the first-hop reflection pulses (1a and 1b) decreases. The time between two reflection pulses (1a and 1b) also decreases. Such relationship is simply determined by the geometry illustrated in Figure 3.4. In fact, the time differences between pulses 0, 1a and 1b are determined by 3-D location of the NBE (x_0, y_0, h) and height of the ionosphere (H). Based on such relationship, we can calculate 3-D location of NBE and ionospheric height using the time differences. In the next chapter, I will analyze such relationship in detail and develop a

method to determine 3-D location of NBE and ionospheric height.

Chapter 4

Discharge height of NBE

4.1 Locating method based on ionospheric reflection of NBE pulse

As introduced in section 3.3, the time difference between direct pulse of NBE and its reflection pulses are determined by 3-D location of the NBE and height of the ionosphere. Based on this mechanism, we can calculate 3-D location of NBE and ionospheric height from these time differences. *Smith et al.* [1999] first used this method to calculate NBE height and ionospheric height. However, this method is only applicable when the distance of the NBE is already known. Here I develop this method to calculate 3-D location of NBE and ionospheric height simultaneously.

Based on the geometric relationship in Figure 3.4, we have the following relations:

$$ct_{ia} = \sqrt{(2H - h - z_i)^2 + r_i^2} - \sqrt{(h - z_i)^2 + r_i^2} \tag{4.1}$$

$$ct_{ib} = \sqrt{(2H + h - z_i)^2 + r_i^2} - \sqrt{(h - z_i)^2 + r_i^2} \tag{4.2}$$

where t_{ia} is the arrival time difference of signal 1a and 0, and t_{ib} is the arrival time difference of signal 1b and 0 in Figure 3.5(a). Both of t_{ia} and t_{ib} can be measured directly from NBE waveforms. r_i is the horizontal distance between the NBE and the ith observation station, given by

$$r_i = R \cdot \arccos\left[\sin(x_0)\sin(x_i) + \cos(x_0)\cos(x_i)\cos(y_0 - y_i)\right] \tag{4.3}$$

where R is the radius of the earth, x_0 and y_0 are the latitude and longitude of the NBE, and x_i and y_i are the latitude and longitude of the i th station.

In equations (4.1) and (4.2) the earth is treated as a flat plane. In this calculation, NBEs with ionospheric reflection pairs are mostly observed between 100 km and 300 km from the network. The ones nearer cannot produce clear reflection pairs and the ones farther cannot be effectively detected. In this range, the error caused by flat earth model is around 100 m, thus can be neglected. Equation (4.3) is based on spherical coordinates rather than Cartesian

coordinates because it turns out that such consideration does not significantly increase the complexity of calculation but it should be closer to the reality.

Substituting equation (4.3) into equations (4.1) and (4.2), the two equations have four unknowns. Each station can provide such two relations, so records of at least two stations can provide a set of solutions. However, it is extremely difficult to solve such nonlinear equations. Therefore I use optimization method to get the solutions. From equations (4.1) and (4.2), I construct the following target function:

$$f(H,h,x_0,y_0)=\sum_{i=1}^{n}\left[ct_{ia}-\sqrt{(2H-h-z_i)^2+r_i^2}+\sqrt{(h-z_i)^2+r_i^2}\right]^2 + \left[ct_{ib}-\sqrt{(2H+h-z_i)^2+r_i^2}+\sqrt{(h-z_i)^2+r_i^2}\right]^2 \tag{4.4}$$

where n is the number of stations observing the same NBE. In this study, every NBE is usually simultaneously observed by 5 or more stations, so optimization method can be used to minimize the function (4.4) and get the solution for 3-D location of NBE (x_0, y_0, h) and ionospheric height (H).

When we get a set of solution (H^*, h^*, x_0^*, y_0^*), the value of function (4.4) is the residual δ_n:

$$\delta_n = f(H^*,h^*,x_0^*,y_0^*) \tag{4.5}$$

We can evaluate the accuracy of the result from the residual. However, this residual is related with the number of stations (n), so it cannot directly show the accuracy of result. Here I construct the residual δ that is not related with n:

$$\delta=\sqrt{\frac{\delta_n}{2n}} \tag{4.6}$$

The value of δ is in meters. When it is smaller than 1000, the error in the result due to computational inaccuracy is smaller than 1000 m and the result is thought relatively accurate.

NBEs located with this method are compared with composite radar reflectivity as shown in Figure 4.1. The storms are nearly 200 km away from the network, and most NBEs correspond well with high reflectivity cores. This result shows that the accuracy of this method is generally satisfactory considering the long distances between the storms and the network and the small area that the network covers.

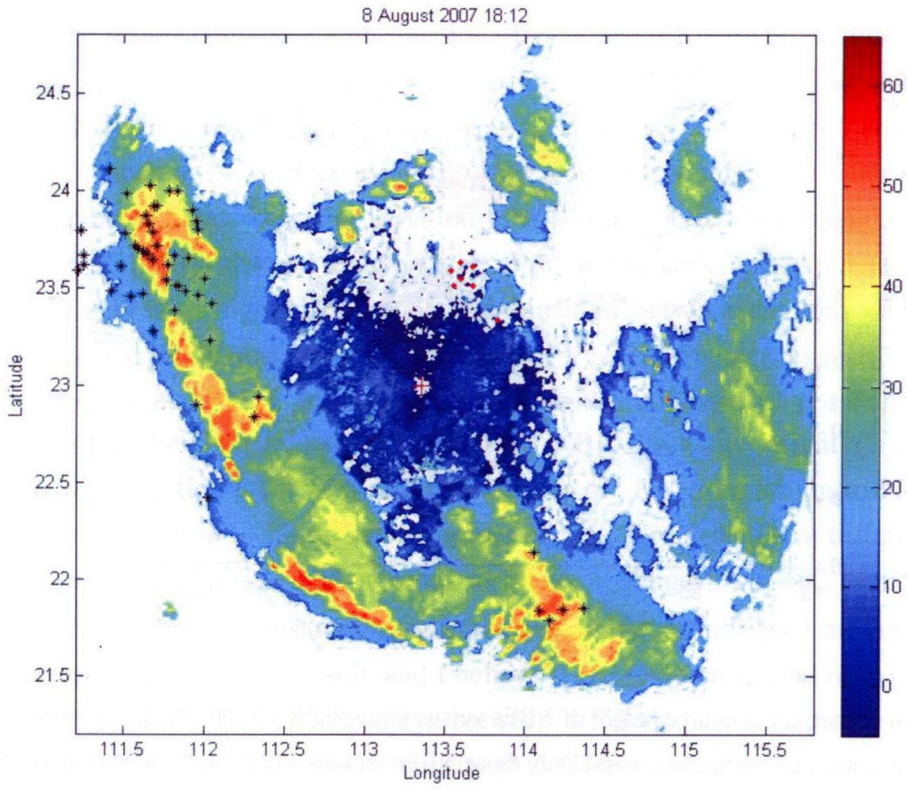

Figure 4.1 Composite radar reflectivity with locations of NBEs within 6 minutes of the radar time. Black "*" represent NBEs, which are located by their ionospheric reflection pairs. Red dots represent observation stations. Red "+" represents the radar station.

Using this method, I calculated the discharge height and ionospheric height of 555 +NBEs and 174 –NBEs in Guangzhou, China, as shown in Figure 4.2. +NBEs and –NBEs show surprisingly distinctive source heights. Heights of most +NBEs ranged from 8 to 16 km, and heights of most –NBEs ranged from 16 to 19 km. This result agrees well with the result of *Smith et al.* [2004], further demonstrating that +NBEs and –NBEs occur in distinctly different altitudes. Ionospheric virtual heights are mostly between 85 km and 95 km. Since NBEs with ionospheric reflection pairs were all observed at night in this study, from about 6 pm to 6 am local time, this result generally agrees with *Smith et al.* [2004] as well.

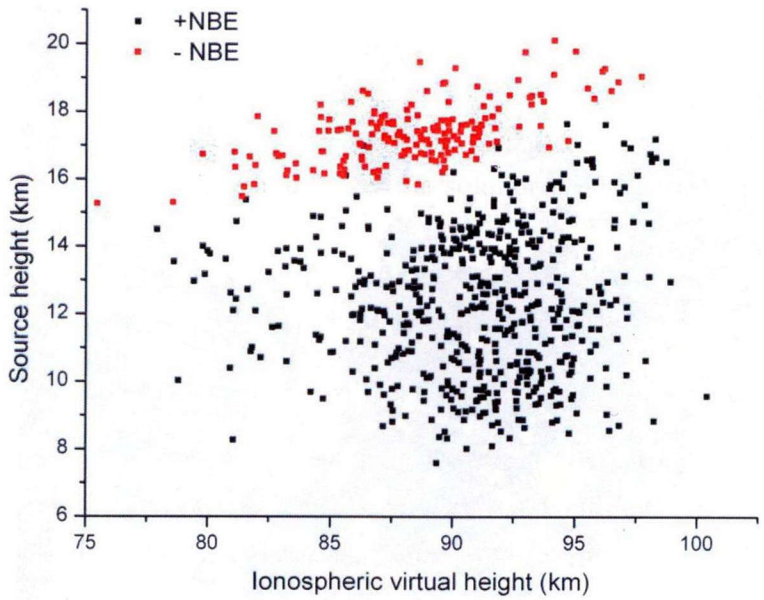

Figure 4.2 A scatterplot of source height of NBEs versus ionospheric virtual height. The results are computed by ionospheric reflection pairs. Only those NBEs located within high reflectivity cores are included.

4.2 Improved method for locating NBE

In most cases, we are only interested in the 3-D location of NBE while the ionospheric height is a known quantity. Therefore, I make a modification to the method in section 4.1, that is, setting the ionospheric height as a constant: $H = H_0 = 90$ km. Therefore the function (4.4) is rewritten as:

$$f(h, x_0, y_0) = \sum_{i=1}^{n} \left[ct_{ia} - \sqrt{(2H_0 - h - z_i)^2 + r_i^2} + \sqrt{(h - z_i)^2 + r_i^2} \right]^2 + \left[ct_{ib} - \sqrt{(2H_0 + h - z_i)^2 + r_i^2} + \sqrt{(h - z_i)^2 + r_i^2} \right]^2 \quad (4.7)$$

Function (4.7) has only three unknowns that determine 3-D location of NBE.

There are two reasons for such a modification. First, with the ionospheric virtual height set as a constant, the number of unknowns decreases from four to three and as a result, the computational accuracy is improved. Figure 4.3(a) and (b) show results of NBE locations computed with function (4.4) and function (4.7), respectively. In Figure 4.3(a), most NBEs are located close to high-reflectivity cores, but some of the location results such as the ones in the white area obviously involve large errors. However, in Figure 4.3(b), almost all NBE

locations are quite well corresponded with high-reflectivity cores, showing much higher accuracy for the results computed with function (4.7). Since the latitude, longitude and height of an NBE are determined simultaneously with function (4.7) using optimization method, it is believable that results of NBE discharge height will also have higher accuracy when computed with function (4.7). Second, NBEs with ionospheric reflection pairs in this study were all observed at night when the variation of the ionospheric virtual height is relatively small. *Smith et al.* [2004] showed that variation of the ionospheric virtual height for radiation waves of NBEs is most significant during the transition between day and night. Relevant studies also showed that ionospheric virtual height at VLF/LF frequencies is around 90 km at night [*Bracewell et al.*, 1951]. In order to determine the influence of possible variation of ionospheric virtual height (H_0) on the result of NBE discharge height (h), I repeated computation with function (4.7) with different choices of H_0 from 85 km to 95 km. Figure 4.4 shows variations of h with different choices of H_0 for 10 NBEs in different altitudes. With ±5-km variation of H_0, variation of the result of h ranges from ±0.27 km to ±0.87 km. Therefore, setting H as a constant will not have a significant influence on the result of h but will increase accuracy of the result, and I believe it is a reasonable treatment.

This method only utilizes time delays between different pulses in the same waveform record, so differences of arrival times of the signal to different observation stations, which are essential in the traditional time-of-arrival technique, are irrelevant with the computation. The error of the computation in this method mainly comes from misidentifications of the reflection pulses, which have been avoided in several ways in this study. First, NBEs far away from the network, which produce polarity reversal of ionospheric reflections or multiple-hop reflections [*Smith et al.*, 2004], are not utilized for computation. In this study, most NBEs producing clear reflection pulses and used for computation are between about 100 km to 300 km from the network. In this range, reflection pulses largely resemble the one in Figure 3.5(a) and are easy to be automatically identified. Second, all the automatic identifications of reflection pulses are manually checked to make sure that there is no apparent misidentification. Such re-examination ensures that there are no large errors in the computation. Finally, the residual of function (4.7) can also indicate error magnitude in the computation, and results with larger-than-normal residuals will be excluded.

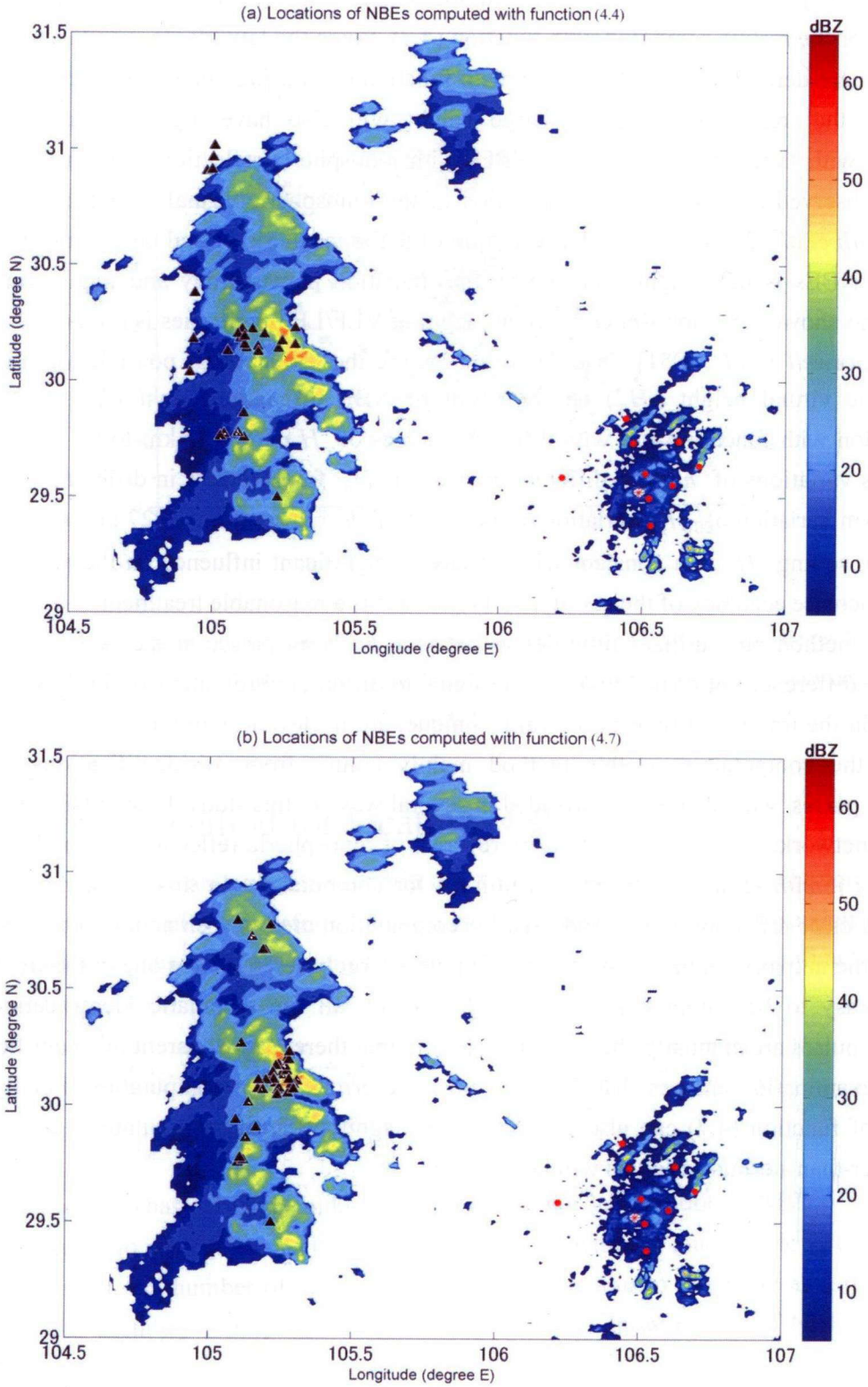

Figure 4.3 Composite radar reflectivity with locations of NBEs within 6 min of the radar scanning time.

Black triangles represent NBE locations computed with their ionospheric reflection pairs using function 4.4 (a) and function 4.7 (b).

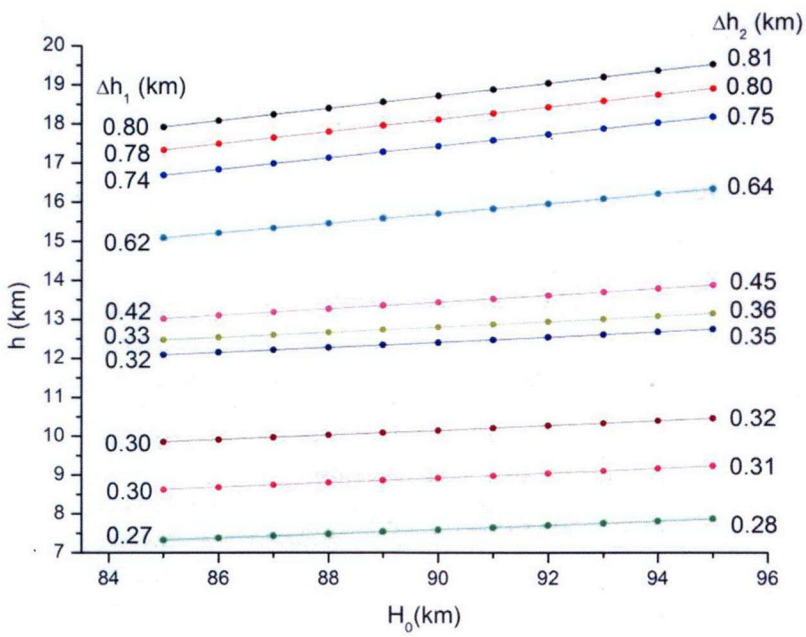

Figure 4.4 Variation of NBE discharge height (h) with different choices of ionospheric virtual height (H_0) for ten NBEs in different altitudes. $\triangle h_1$ is difference between results of h computed with H_0=90 km and H_0=85 km. Δh_2 is difference between results of h computed with H_0=95 km and H_0=90 km.

In order to estimate errors in the results of NBE discharge height due to inaccuracy in determining reflection pulses, I made the following test. For a typical NBE observed by five stations, up to 4-μs error is intentionally added in the identification of ionospheric reflection pulse recorded by two of the five stations. Under such condition, 2-D location (latitude and longitude) of the NBE is up to 40 km from the original position, which is a significant error. However, the height result shows no larger than 0.5-km variance from the original result, indicating that the height result is much more stable than the results of latitude and longitude. This can also be qualitatively seen from function (4.7), in which r_i, determined by latitude (x_0) and longitude (y_0) of NBE, is a much larger quantity (~200 km) than the height (h, ~15 km). The value of r_i (and the value of x_0 and y_0), therefore, has the largest variation through the process of searching the minimum of the function, while the value of h has relatively small variation. For the same reason, if function (4.4) is utilized, results of ionospheric virtual height (H, ~90 km) will also have relatively large variations (Figure 4.2). Since errors in 2-D locations of NBEs rarely exceed 40 km according to comparisons of NBE locations with radar reflectivity, errors in discharge heights of NBEs due to inaccuracies in determining reflection pulses are generally smaller than 0.5 km.

4.3 Statistical results of NBE discharge height

With the method introduced in section 4.2, discharge heights of thousands of NBEs in Guangzhou and Chongqing were calculated. In Guangzhou, there are a total of 1318 and 625 height results for +NBEs and –NBEs. The geometric means (GMs) of discharge height are 12.1 km and 17.3 km, and the arithmetic means (AMs) are 12.3 km and 17.3 km. In Chongqing, there are a total of 5489 and 1400 height results for +NBEs and –NBEs with GMs of 9.9 km and 17.5 km and AMs of 10.0 km and 17.5 km, respectively. Statistics of discharge height of NBEs observed in these two regions are summarized in Table 4.1. All the results are given as above ground level (AGL), but they should not have much difference with the heights above mean sea level (AMSL) because all station elevations in Guangzhou are smaller than 100 m and the ones in Chongqing are mostly around 300 m.

Table 4.1 Statistics of Discharge Height of NBEs

		Number	GM (km)	AM (km)	Maximum (km)	Minimum (km)
Guangzhou	+NBE	1318	12.1	12.3	17.5	7.0
	–NBE	625	17.3	17.3	19.6	14.6
Chongqing	+NBE	5489	9.9	10.0	17.8	6.4
	–NBE	1400	17.5	17.5	19.9	7.0

Figure 4.5 shows distributions of discharge heights of NBEs observed in Guangzhou and Chongqing. It clearly shows that +NBEs and –NBEs occur in two different altitudes, with –NBEs mostly higher than +NBEs. Most +NBEs occur between 8 and 16 km while most –NBEs occur between 16 and 19 km in Guangzhou. The distribution in Chongqing is quite similar, with +NBEs converging in lower altitudes compared with that in Guangzhou. Such distribution is also consistent with the result of *Smith et al.* [2004], further confirming that –NBEs occur at a region higher than +NBEs.

An interesting result in my calculations is that very few NBEs are above 19 km as shown in the height distribution in Figure 4.5. As summarized in Table 4.1, the highest NBE in Guangzhou is 19.6 km, and the highest one in Chongqing is 19.9 km. However, there are only 6 NBEs (0.31%) in Guangzhou and 18 NBEs (0.26%) in Chongqing above 19 km, all of which are negative polarity. The majority of –NBEs occur between 16 km and 19 km with a peak between 17 and 18 km, both in Guangzhou and Chongqing. The result given by *Smith et al.* [2004] also showed a peak around 17 km in height distribution of –NBEs (see their Figure 5). According to their distribution curve, which shows a sudden decrease above 20 km, it seems very likely that most NBEs above 20 km are resulted from errors probably caused by misidentifications of reflection pulses in their automatic identification routine. *Nag et al.*

[2010] also showed several +NBEs that were above 20 km. In our study, the maximum heights of +NBEs are 17.5 km and 17.8 km, respectively, in Guangzhou and Chongqing, and the majority of +NBEs are below 15 km. *Smith et al.* [2004] also showed very few +NBEs were above 17 km. Considering their very small sample (48 +NBEs), it seems that results of +NBEs above 20 km in *Nag et al.* [2010] may due to computational errors.

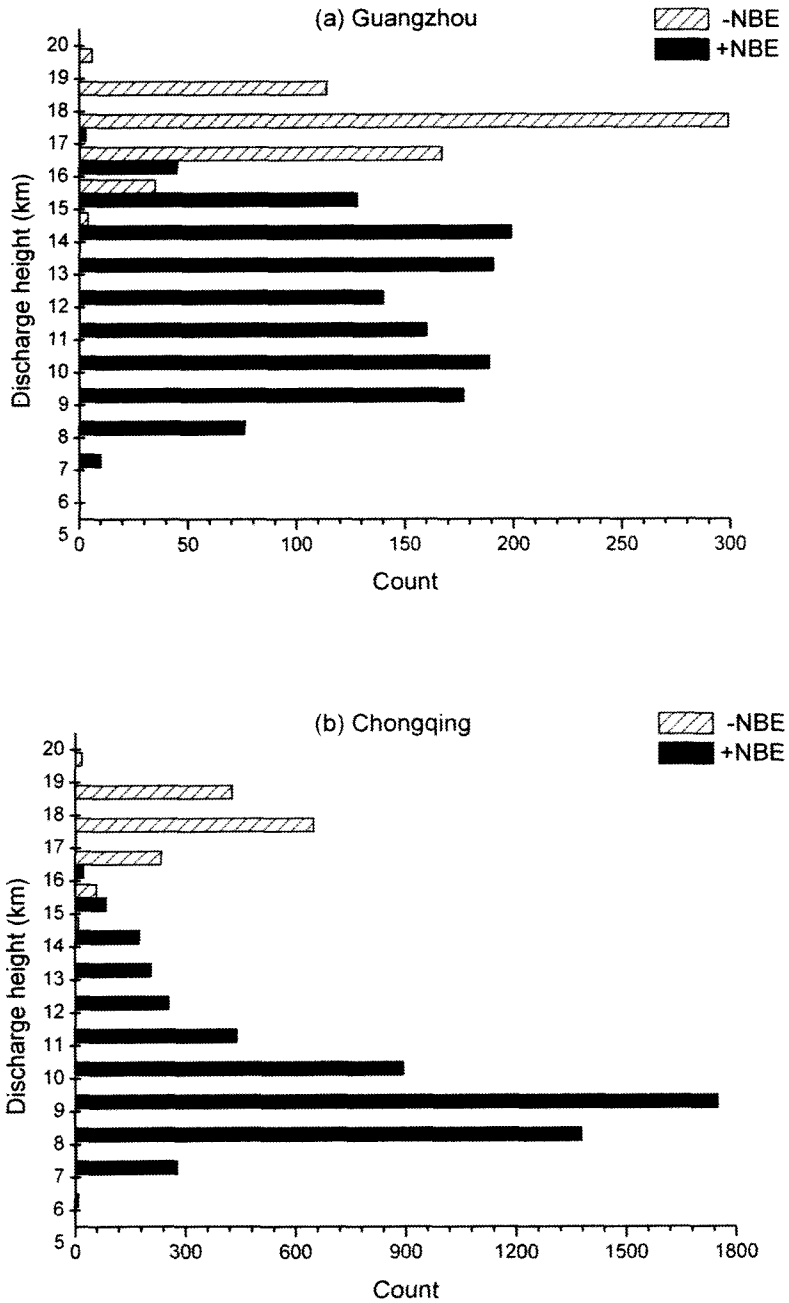

Figure 4.5 Distributions of discharge heights of NBEs observed in (a) Guangzhou and (b) Chongqing.

The minimum height of –NBE in Chongqing is 7.0 km, much smaller than that in Guangzhou. However, there are only 5 –NBEs (0.073%) below 14 km in Chongqing, among which 2 were around 12 km and 3 were from 7 to 7.5 km. Other than these 5 cases, the minimum height of –NBE in Chongqing is 14.1 km, similar to that in Guangzhou. As for the five –NBEs with exceptionally low height, I checked their waveforms and re-examined the computation procedure, and I believe the height results are accurate. However, I am not sure whether they are truly NBEs, which produce not only narrow and bipolar pulses in low frequency radio bands but also very strong radiation in high frequency radio bands. It is possible that they are polarity-inverted intracloud discharges produced below the main negative charge layer [*Qie et al.,* 2005]. Such intracloud discharges may produce large bipolar electric field change waveforms that are similar to NBEs. Since we do not have observations in VHF bands to help identify NBEs, such misidentification is possible. Even if they are truly NBEs, they should have some special characteristics or are produced in special conditions as they are significantly lower than other –NBEs and only account for an extremely small percent (0.073%).

In summary, we state that –NBEs mostly occur between 16 and 19 km; few are above 19 km or below 14 km. +NBEs occur in a wider range, mostly between 7 and 16 km. On the basis of discharge height distributions and discharge polarities, I conclude that +NBEs are probably produced between the main negative charge layer and the upper positive charge layer while –NBEs are probably produced between the upper positive charge layer and the screening negative charge layer at the cloud top as roughly illustrated by Figure 4.6. Such a charge structure is consistent with typical charge distributions in updraft regions of thunderstorms [*Stolzenburg et al.,* 1998].

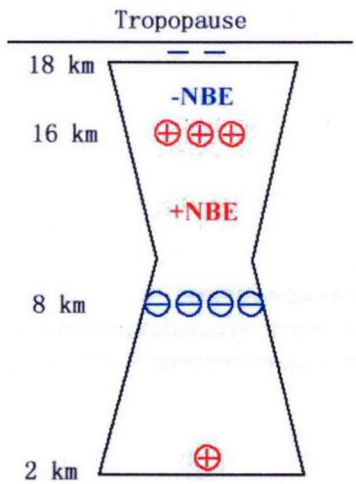

Figure 4.6 Illustration of discharge heights of +NBE and –NBE with respect to the charge layers in a thunderstorm.

4.4 Variation of NBE discharge height in thunderstorms

Fierro et al. [2011] discussed variation of NBE discharge heights in Hurricanes Rita and Katrina, but NBEs in their study were all positive polarity. Here we present the first analysis of height variations of both polarities of NBEs in two thunderstorms. Both of these two thunderstorms occurred at night with a distance of about 200 km from the lightning location network, so most of NBEs were recorded with well-defined ionospheric reflection pairs and could be located with the method introduced in section 4.2. Although radar observations of these two thunderstorms are available, which can be used to relate NBEs with the thunderstorm producing them, the radar stations were too far away in most periods of the thunderstorms and therefore could not give accurate information on the structure of the thunderstorms.

The first thunderstorm was observed in Chongqing, which was the only one in the observation in Chongqing that produced more –NBEs than +NBEs. As in Figure 4.7, there are 615 +NBEs and 1108 –NBEs, most of which are produced in the period from 23:30 to 02:30.

Similar to the height distribution in Figure 4.5(b), height of +NBE shows a much larger variation than that of –NBE. In the period from 00:00 to 02:00, height variations of +NBEs are as large as 8 km in several minutes. *Fierro et al.* [2011] shows that in each NBE burst in Hurricanes Rita and Katrina, height variations of +NBEs are only 2 to 3 km. However, at the end of the Hurricane Rita, the height variation is as large as 12 km (see their Figure 3), very similar to my result. The reason for such large height variation is currently unknown. It may be simply because NBEs can be produced in any place between corresponding charge layers as illustrated in Figure 4.6. Relatively small height variations of –NBEs indicate narrow space between upper positive charge layer and the screening charge layer. It is also reported that these two charge layers are sometimes partially mixed with each other [*Riousset et al., 2010*].

Each 15 successive +NBEs and –NBEs, respectively, are grouped together (the last group may contain less than 15 +NBEs or –NBEs), and the average height of each group is computed and represented by blue and green triangles in Figure 4.7. The density of triangles can also indicate NBE rate. Rate of +NBE and –NBE generally correspond with each other, both of which reach very large values in the period from about 00:00 to 02:00. In this period, a considerable amount of +NBEs are occurring at relatively large heights (above 13 km). At the end of this thunderstorm (after about 03:00), few –NBEs are produced, and all +NBEs are occurring at lower heights (no +NBE is above 10 km after 03:00). In the periods when no –NBE is produced (indicated by shaded rectangles in Figure 4.7), there are 87 +NBEs with an average height of 10.1 km, while in the periods with –NBEs, there are 528 +NBEs with an average height of 11.0 km. So +NBEs are generally higher when –NBEs are produced at the same time.

The black curve in Figure 4.7 divides +NBEs and –NBEs into two sides, representing possible heights of the upper positive charge layer (see charge structure in Figure 4.6). It is interesting to note that all –NBEs are above the curve and all but two +NBEs are below the curve, indicating that –NBEs are always above +NBEs at the same moment, consistent with the charge structure for NBE productions in Figure 4.6. It also indicates that height results in Figure 4.7 do not have significant errors, otherwise there should be at least some +NBEs and –NBEs mixed together and it would be impossible to draw such a dividing curve.

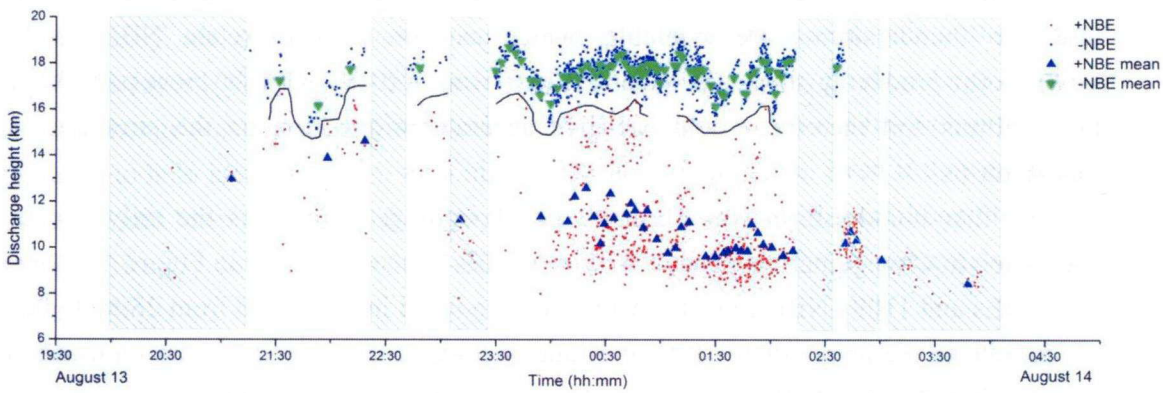

Figure 4.7 NBE discharge heights in a thunderstorm in Chongqing. Blue and green triangles represent average heights for each 15 successive +NBEs and –NBEs, respectively. Shaded rectangles indicate the periods when no –NBE is produced. Black curve represents the possible location of the upper positive charge layer, dividing almost all +NBEs and –NBEs into two sides.

The second thunderstorm was observed in Guangzhou, which was predominated by +NBEs. As shown in Figure 4.8, –NBEs are only produced in a short period. There are a total of 262 +NBEs and 69 –NBEs in Figure 4.8. Similar to the case in Figure 4.7, height variations of +NBEs are very large, about 6 km in several minutes. The NBE production shows 3 bursts in this case in which relatively large number of NBEs are produced in short intervals, similar to that shown by *Fierro et al.* [2011]. In the burst 2, –NBEs were also produced, and the overall height of +NBEs in this period is larger than that in other periods. In the periods when no –NBE is produced (indicated by shaded rectangles in Figure 4.8), the average height of +NBEs is 12.7 km, much smaller than that in the periods with –NBEs, which is 15.0 km. The black curve has the same function as in Figure 4.7. Note that all +NBEs are below the curve and all but 1 –NBE are above the curve.

Summarizing the above two cases, we have the following conclusions. First, NBEs seem to be able to occur in any position between corresponding charge layers, making height variations very large in most periods of a thunderstorm, especially for +NBEs. However, at the end of a thunderstorm, when elevations of charge layers are probably decreasing, heights of NBEs are also decreasing and usually have small variations. Second, discharge heights of

+NBEs are generally higher when –NBEs are occurring in the same period. This indicates that when –NBEs are occurring, updraft is stronger, lifting charge layers responsible for +NBE production to a larger altitude. Third, for a given short time period in a single storm, –NBEs are always observed to occur at a higher altitude than +NBEs, supporting the conclusion that +NBEs are below the upper positive charge layer while –NBEs are above the upper positive charge layer.

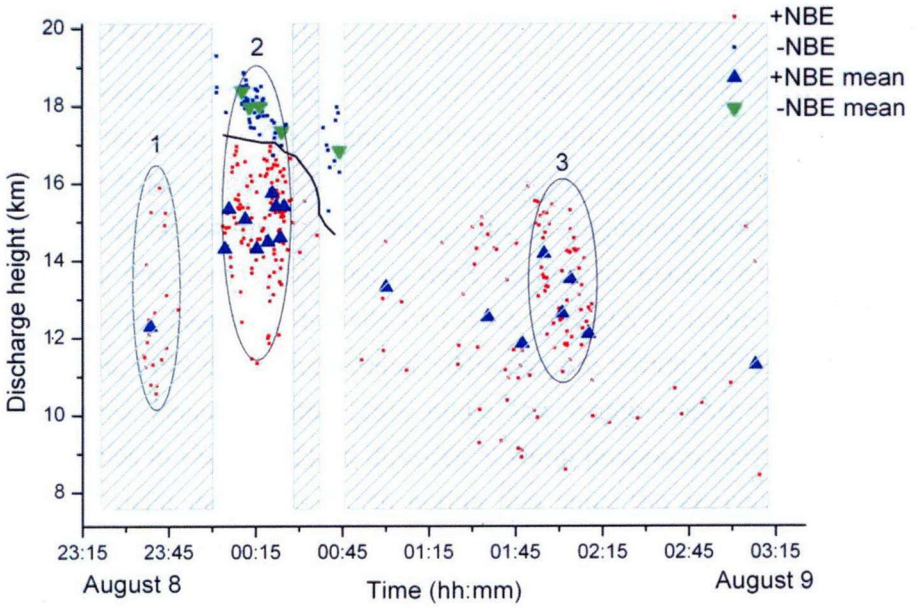

Figure 4.8 As in Figure 4.7, but for a thunderstorm in Guangzhou. The black ovals labeled 1 to 3 highlight NBE bursts.

Chapter 5

Relationship between NBE and thunderstorm

5.1 Statistical relationship

Here I first present a statistical analysis on the relationship between NBE and thunderstorm using the data in Guangzhou, China. In this region, large number of both positive and negative NBEs were observed, so it is useful for analyzing different behaviors of +NBE and –NBE in thunderstorm. In this region, the LF lightning location system covers a quite small region so the observation area is quite limited comparing with previous studies [e.g., *Wiens et al.*, 2008] based on the data of LASA. In order to relate the NBEs with the storm producing them, only those storms and NBEs that are within 150 km from the central station are considered because within this range the location error is relatively small (indicated by red circles in Figure 5.1). In this area, 9 storm processes are conveniently picked out according to the radar data. It is worth noting that since the analysis area is relatively small, the storm processes considered are not always the entire storm processes, that is, a storm may not be formed within the area or may move out of the area in its later stage. In order to statistically study the relationship between NBEs and convective strength, the time of each storm is divided into windows of duration of 6 min, equivalent to the time separation of radar's volume scans. But the area is not divided into equivalent grids like previous studies. Instead, only when the area comprises multiple independent storms and each storm produces NBEs is the area separated into multiple zones to ensure that each zone covers a separate storm, otherwise the whole area is considered as a single zone. Each zone is treated as a data cell, and the number of both +NBEs and –NBEs and the maximum reflectivity of this data cell are calculated. For example, in Figure 5.1(a), only one data cell is considered, while in Figure 5.1(b), two data cells are considered (illustrated by black circles in Figure 5.1). In this way, a total of 698 data cells are obtained.

Unlike previous studies, such a procedure creates data cells that do not have identical areas, but the areas usually do not differ a lot, and when the ratio of +NBEs to –NBEs is considered, difference of areas is not a problem. An obvious advantage of this procedure is that each data cell contains a separate storm and a single storm would not be divided into multiple data cells.

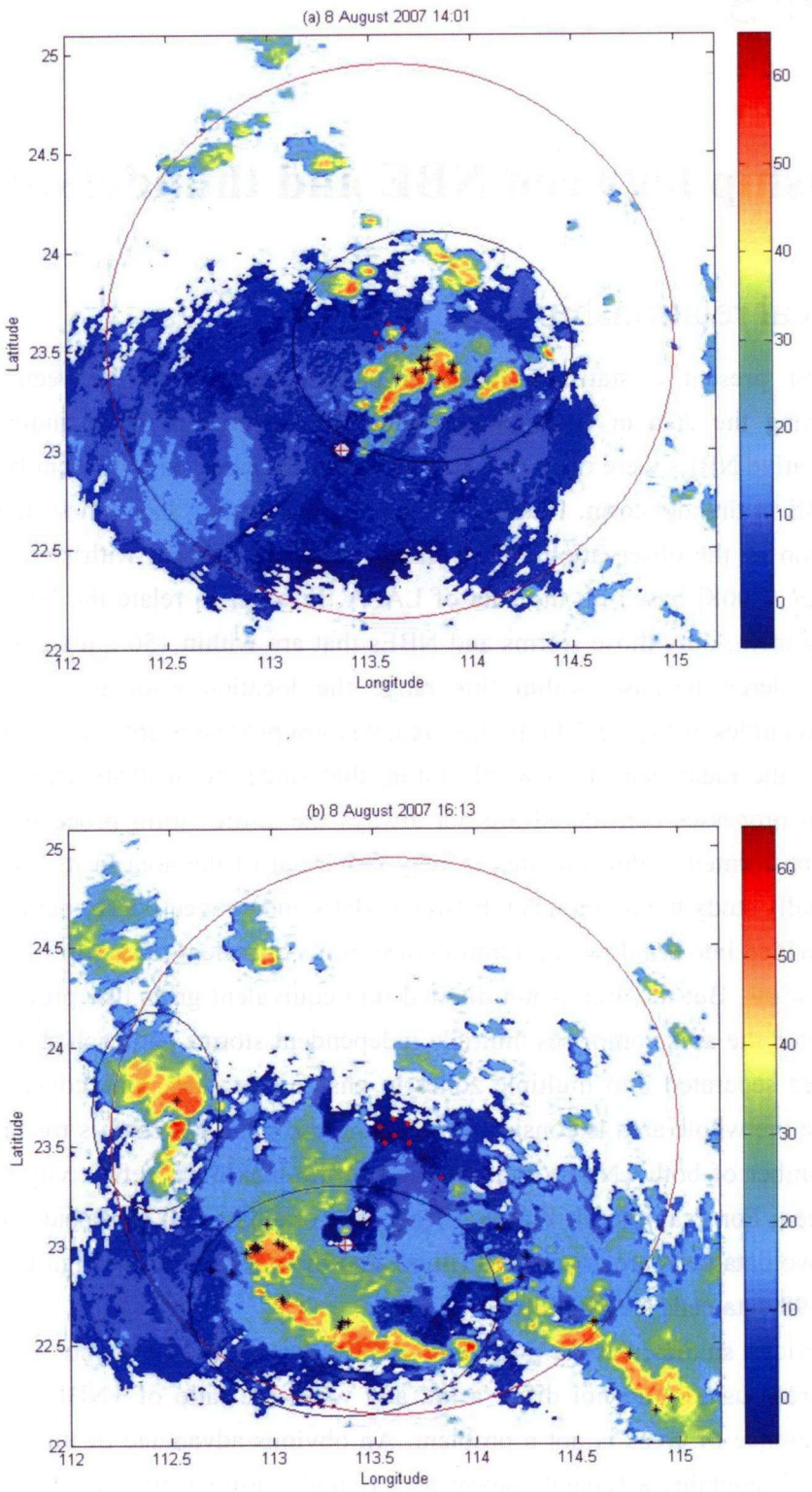

Figure 5.1 Composite radar reflectivity with locations of NBEs within 6 minutes of the radar time. Red dots

represent observation stations. Red "+" represents the radar station. Black "*" represent NBEs. The red circle represents an equidistance of about 150 km from the central station. Black circles are to illustrate the cell-creation procedure.

In all of 698 data cells, 416 have at least one NBE. The number of NBEs and the maximum reflectivity of each data cell are scatter-plotted in Figure 5.2. The red line connects the average number of NBEs with the same value of maximum reflectivity. The maximum reflectivity is obviously correlated with convective strength to some degree and has been employed by *Wiens et al.* [2008] to infer the relationship between NBEs and convective strength as well. Note that radar-derived storm top is not utilized here because the value is seriously inaccurate when the storm is very near the radar station. Figure 5.2 shows that the average NBE rate increases with the maximum reflectivity of smaller than 58 dBZ. The large variation of NBE rates when the maximum reflectivity is larger than 58 dBZ is probably because of small sample of data cells. This result is in accordance with previous studies [e.g., *Wiens et al.*, 2008] and also justifies this cell-creation procedure in this study.

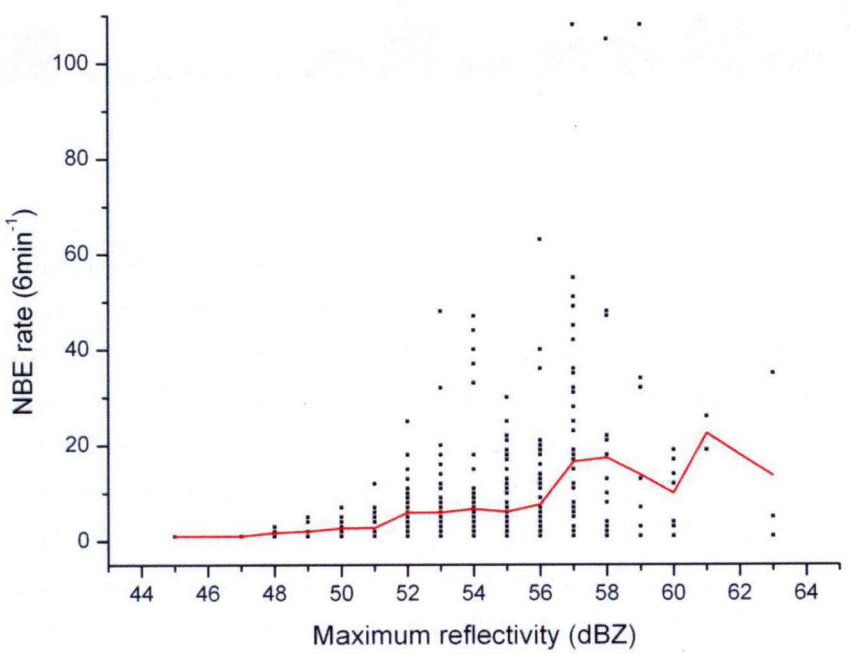

Figure 5.2 A scatterplot of NBE rate versus maximum reflectivity for each data cell. The red line connects the mean value of NBE rate of each value of maximum reflectivity.

Figure 5.3 shows the distribution of percentages of –NBEs of each data cell. A pronouncing feature in Figure 5.3 is that there are 218 data cells having only +NBEs, accounting for 52.4% of all data cells with at least one NBE. Besides, 29 data cells have only –NBEs. The number of data cells with only one polarity NBEs is 247, accounting for 59.4%

of all data cells with at least one NBE. From another perspective, the percentages of –NBEs in 9 storms in this study are 40.7%, 54.2%, 13.2%, 17.6%, 15.1%, 41.4%, 27.1%, 35.0%, 9.5%, respectively. Clearly most storms have more +NBEs than –NBEs, and both polarities of NBEs occur in the same storm. These results indicate that on a small time scale (6 min in this study), NBEs tend to occur as the same polarity; that is, NBEs of the same polarity tend to cluster in a short period. However, on the time scale of a storm, NBEs of both polarities are produced.

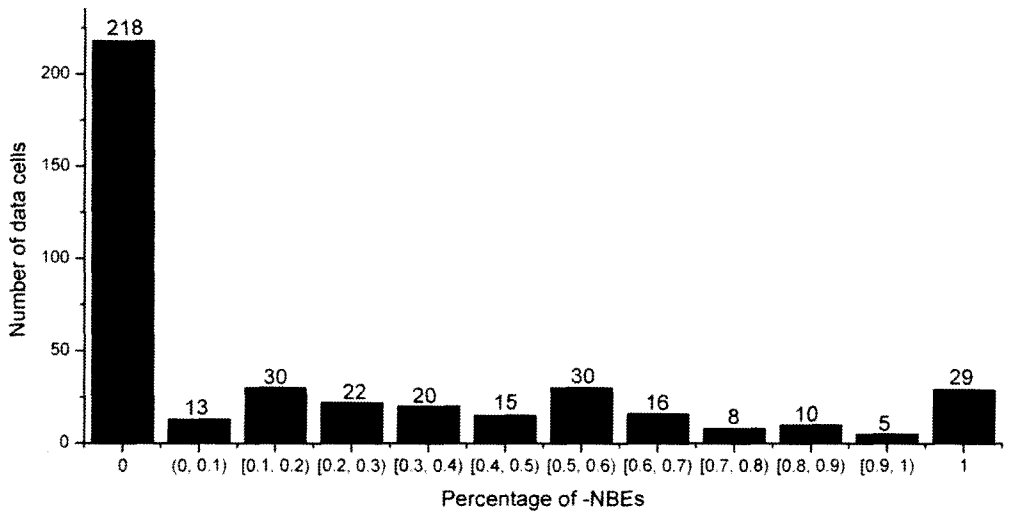

Figure 5.3 Distribution of percentages of –NBEs in each data cell.

Jacobson and Heavner [2005] and *Wiens et al.* [2008] have both statistically studied the ratio of +NBEs to –NBEs in a given storm. *Jacobson and Heavner* [2005], on the basis of LASA observation in Florida, found that a given storm rarely produced both polarities of NBEs. However, *Wiens et al.* [2008] found that both polarities of NBEs often occurred in the same storm in Great Plains. *Hamlin et al.* [2009] stated that the difference of NBE production in Great Plains versus Florida possibly indicated the difference in the storms themselves. However, it should be noted that both analyses by *Jacobson and Heavner* [2005] and *Wiens et al.* [2008] were based on grid cells having duration of 10 min. Here I have demonstrated that at a short time scale NBEs tend to be of single polarity. As shown above, 59.4% of data cells have only one polarity of NBEs, which is likely corresponding to the result of *Jacobson and Heavner* [2005]. It seems that both of the above analyses could only show the ratio of +NBEs to –NBEs at a time scale of 10 min instead of a given storm. For 9 storms in this study, every storm produces both polarities of NBEs, and it is very likely that for a given storm in both of Florida and Great Plain, it also produces both polarities of NBEs.

Although +NBEs are more prevalent, the biggest number of –NBEs in one data cell is larger than that of +NBEs. The three largest numbers of –NBEs in one data cell are 95, 71,

and 51. And the three largest numbers of +NBEs in one data cell are 67, 48, and 46. Three data cells have total duration of only 18 min, but they account for 19.41% and 7.22%, respectively, of all –NBEs and +NBEs. This clearly demonstrates the temporal compactness of NBE occurrences, which has also been pointed out by previous studies [e.g., *Jacobson and Heavner,* 2005]. And this result indicates that –NBEs are more pronounced than +NBEs in such characteristic.

Percentage of –NBEs in each storm varies considerably, from 9.5% to 54.2%. It seems that the percentage of –NBEs in a storm is connected with the convective strength. Figure 5.4 depicts the mean maximum reflectivity versus the percentage of –NBEs in each storm, and they are linearly fitted with a correlation coefficient of 0.62. The mean maximum reflectivity is calculated by averaging the maximum reflectivity of all data cells in a given storm. The trend for the mean maximum reflectivity to increase with the percentage of –NBEs is obvious. This result probably has certain associations with the fact that the heights of –NBEs are mostly larger than that of +NBEs. Since maximum reflectivity is related with convective strength and height of cloud top to some degree, this result may indicate that the higher a thunderstorm develops the greater possibility it has to produce –NBEs.

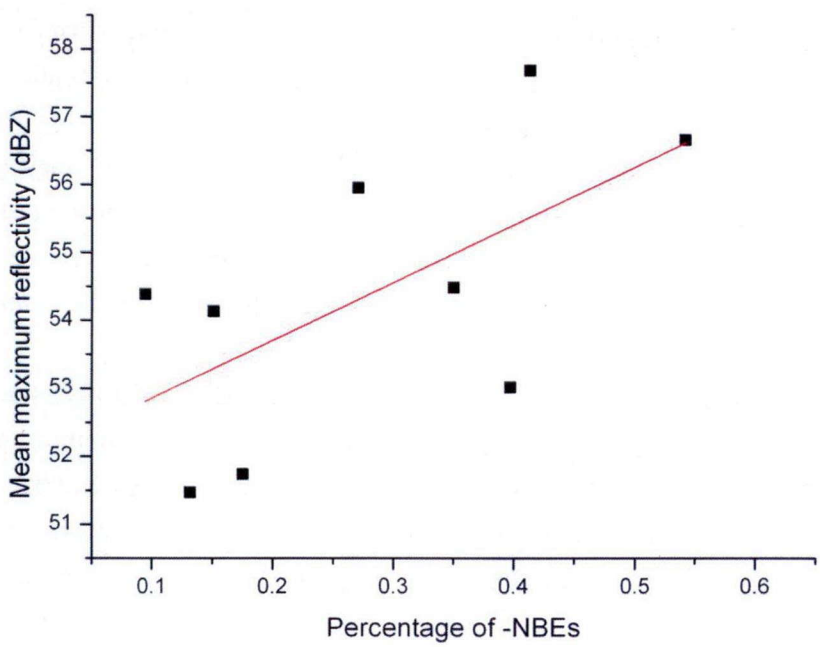

Figure 5.4 A scatterplot of the mean maximum reflectivity versus percentage of –NBEs in each storm. The mean maximum reflectivity is calculated by averaging the maximum reflectivity of all data cells in a given storm.

5.2 NBE location relative to a thundercloud

In Chapter 4, I have demonstrated that +NBE and –NBE are associated with different charge layers. +NBE is produced between the main negative charge layer and the upper positive charge layer while –NBE is produced between the upper positive charge layer and the negative screening charge layer (Figure 4.6). However, discharge heights of some –NBEs are estimated to be significantly higher than the tropopause [*Smith et al.*, 2004; *Nag et al.*, 2010], which is difficult to understand because thundercloud has little chance to develop to such height. In my calculation of NBE height in Chapter 4, I showed that no NBE is higher than 20 km, and extremely large results in previous studies are probably due to computation errors. However, so far there is still no direct evidence to prove that –NBEs, occurring higher than 15 km or even close to 20 km, are inside thundercloud.

With the observation of PAR with very high temporal and spatial resolution as well as LF lightning location system in Osaka region, we have the first chance to reveal NBE location relative to a thundercloud.

5.2.1 Horizontal structure

First I compare NBE location with horizontal structure of thunderstorm to examine whether NBEs always correspond to the most vigorous region of thunderstorm. Locations of NBEs usually correspond well with the region of strongest convection (indicated by the largest 20-dBZ height) as shown in Figure 5.5(a) and 5.5(b). In Figure 5.5(a) the 20-dBZ height is 9.0 km and NBE height is 5.9 km. In Figure 5.5(b), the 20-dBZ height is 13.6 km and NBE height is 10.7 km. The region where NBE is produced has the largest cloud top height at that moment. It appears that NBE is selective for the deepest convection. Such corresponding relationship has been suggested and reported by many studies [*Jacobson and Heavner*, 2005; *Wiens et al.*, 2008].

However, the actual situation is more complicated. Figure 5.5(c)-(f) are from two independent thunderstorms on August 14, 2012. Cloud tops of these two thunderstorms stayed higher than 15 km for a long time, which is not common in Osaka region. These two thunderstorms produced 150 +NBEs (65%) and 11 –NBEs (50%). +NBEs in these two thunderstorms are apparently not selective for the deepest convection; instead, they converge around, and outside of, the region with deepest convection. In Figure 5.5(c) and 5.5(d), locations of several +NBEs form a circle right around the region with the highest cloud top, and all NBEs are located in regions with 20-dBZ height lower than 15 km. In Figure 5.5(e), four +NBEs are located at one side of the 15-km contour. In Figure 5.5(f), two –NBEs (with the same location, also shown in Figure 5.6(d)) are located almost right at the center of the thunderstorm, but seven +NBEs are scattered near the edge of the thunderstorm. Such feature

can also be found in other thunderstorms, but it seems most pronounced in very deep convections.

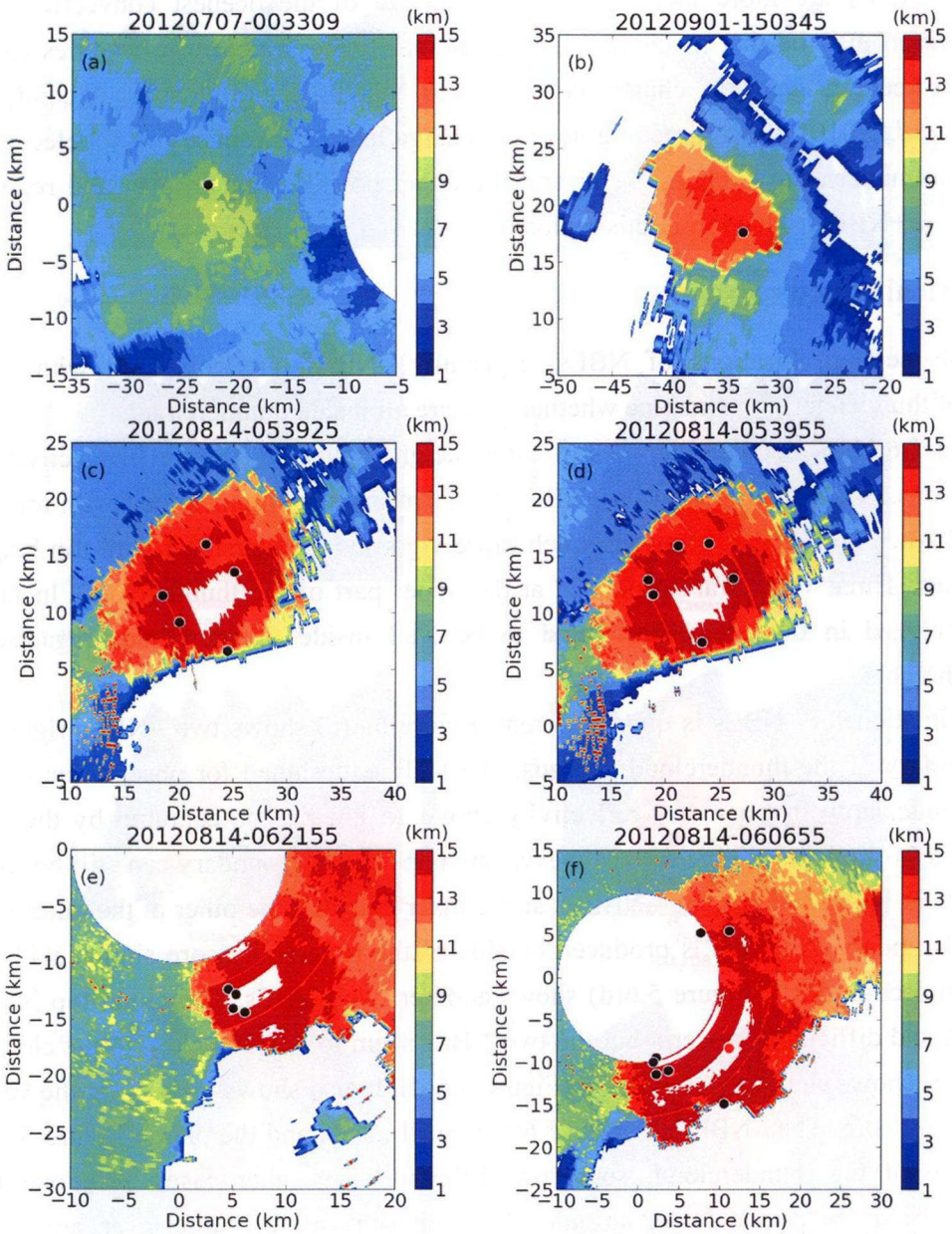

Figure 5.5 Height of 20 dBZ calculated from PAR reflectivity data. The PAR is located at (0, 0). Black points represent +NBEs and red points represent –NBEs within ±15 seconds of the radar time.

One possible explanation for such phenomenon is that under intense updraft, ice crystals with positive charges are elevated to a higher altitude while graupels (larger and heavier) carrying negative charges still stay in the mixed-phase region, thus reducing electric field between these two charge layers, which are responsible for the production of +NBEs. Therefore +NBEs are more inclined to occur outside of the deepest convective region. Another reason may be that as cloud top extends into higher altitude, it becomes easier to form the screening negative charge layer due to increase of atmospheric conductivity [*Riousset et al.*, 2010]. Such screening negative charge layer can reduce the net electric field between the main negative charge layer and the upper positive charge layer and reduce the possibility of +NBE production in this region.

5.2.2 Vertical structure

In this section, locations of NBEs, especially –NBEs, are compared with vertical structure of thunderstorm to examine whether they are all inside thundercloud.

Figure 5.6 shows some examples of range-height indicator (RHI) of reflectivity with NBE locations. Figure 5.6(a) shows a +NBE of 5.7 km inside a thundercloud with top height of about 9 km. Figure 5.6(b) shows a much more vigorous thunderstorm with top height of about 14 km. Three +NBEs are produced at the upper part of the thundercloud. In fact, all +NBEs analyzed in this study are found to be well inside thunderclouds regardless of storm-top heights.

The situation for –NBEs is quite different. Figure 5.6(c) shows two –NBEs right at the upper boundary of the thundercloud. Because the PAR is designed for observation of up to 15-km altitude, only fragments of reflectivity above 15 km can be captured by the end of some beams as shown in Figure 5.6. However, the upper cloud boundary can still be roughly figured out. In Figure 5.6(c), one –NBE is at the inner side and the other at the outer side of the upper boundary. A +NBE is produced outside of the reflectivity core similar with those analyzed in section 5.2.1. Figure 5.6(d) shows another two –NBEs. The cloud top is higher than 15 km and difficult to discern, but the two NBEs seem to be quite close to the cloud top. Figure 5.6(e) shows similar situation with Figure 5.6(d). It also shows a +NBE at the verge of the reflectivity core. The –NBE in Figure 5.6(f) is well inside and the one in Figure 5.6(g) is well outside of the thundercloud, somehow different from other cases. The one inside thundercloud may be due to lower altitude of the upper positive charge layer, and the one outside thundercloud may be due to transient overshooting that is not captured by the PAR. Figure 5.6(h) shows a very low –NBE (13.3 km), which is also right at the top of the thundercloud.

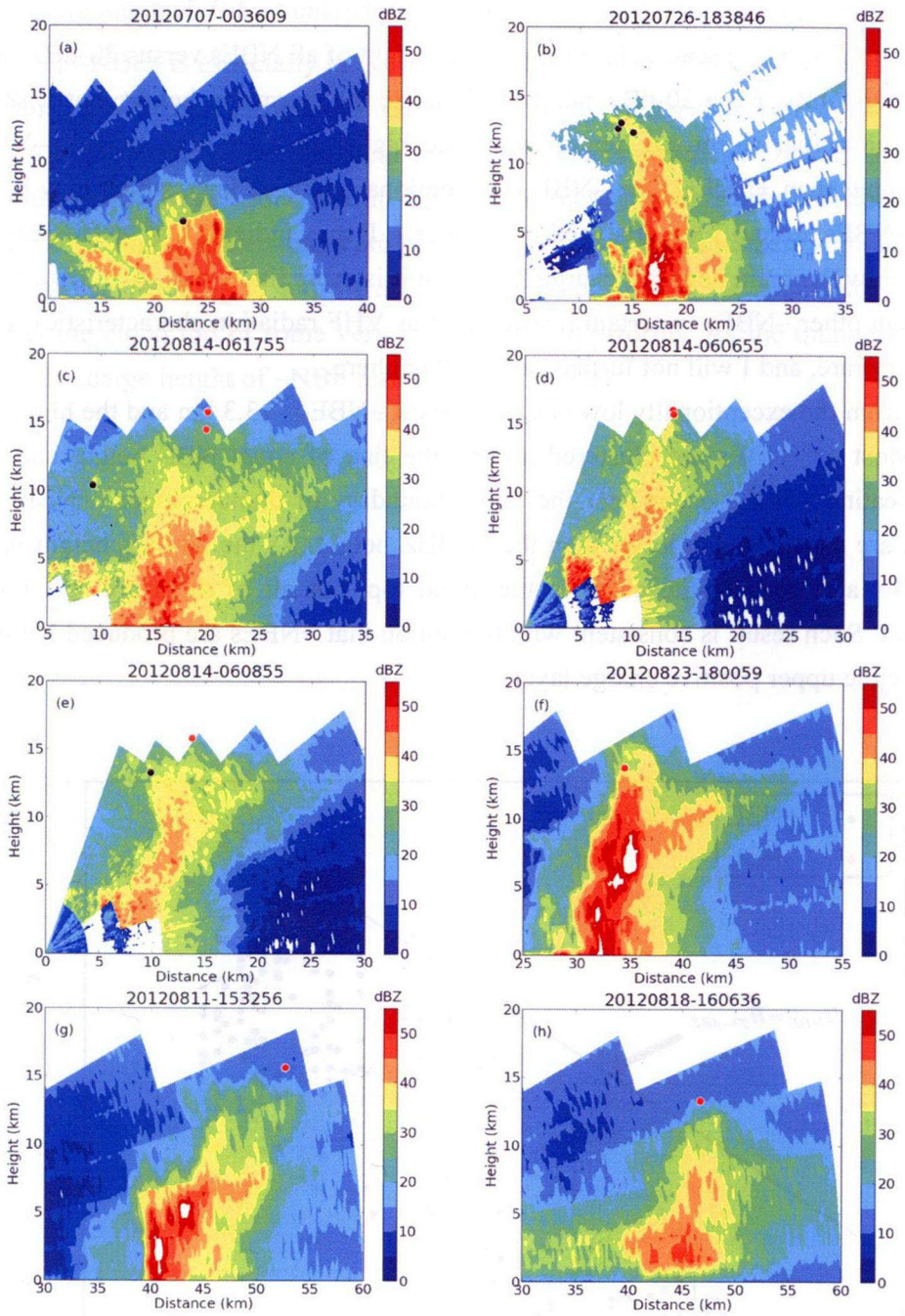

Figure 5.6 RHI of reflectivity observed by the PAR. The PAR is located at (0, 0). Black points represent

+NBEs and red points represent –NBEs within ±15 seconds of the radar time.

In summary, +NBEs are always well inside thundercloud while –NBEs are usually at the upper boundary of the thundercloud. Sometimes –NBEs are at the inner side of the boundary while sometimes they are at the outer side, which may be due to different situations analyzed above. Figure 5.7 shows a scatterplot of discharge height of all NBEs versus 20-dBZ height of parent thunderstorms. I use 20-dBZ height to indicate the storm top height, but it should be noted that the actual storm-top height is a little higher than 20-dBZ height. –NBEs are generally higher than +NBEs. One –NBE is exceptional low (8.1 km), which may be similar with three –NBEs around 7 km analyzed in Chapter 4. It may indicate that –NBEs can also be produced below the main negative charge layer, but it is more likely that such low –NBEs are different from other –NBEs in certain respect such as VHF radiation characteristics. But such cases are very rare, and I will not further discuss them here.

Apart from the exceptionally low one, the lowest –NBE is 13.3 km and the highest one is 16.0 km. Most of –NBEs are clustered around the line of equal NBE height and 20-dBZ height, indicating –NBEs occur near the upper boundary of thunderclouds. +NBEs, on the other hand, are usually much lower than the 20-dBZ height. As the 20-dBZ height increases, some +NBEs also reach quite close to the cloud top, but all of them are still inside the thundercloud. Such result is consistent with the notion that +NBEs are produced below and –NBEs above the upper positive charge layer.

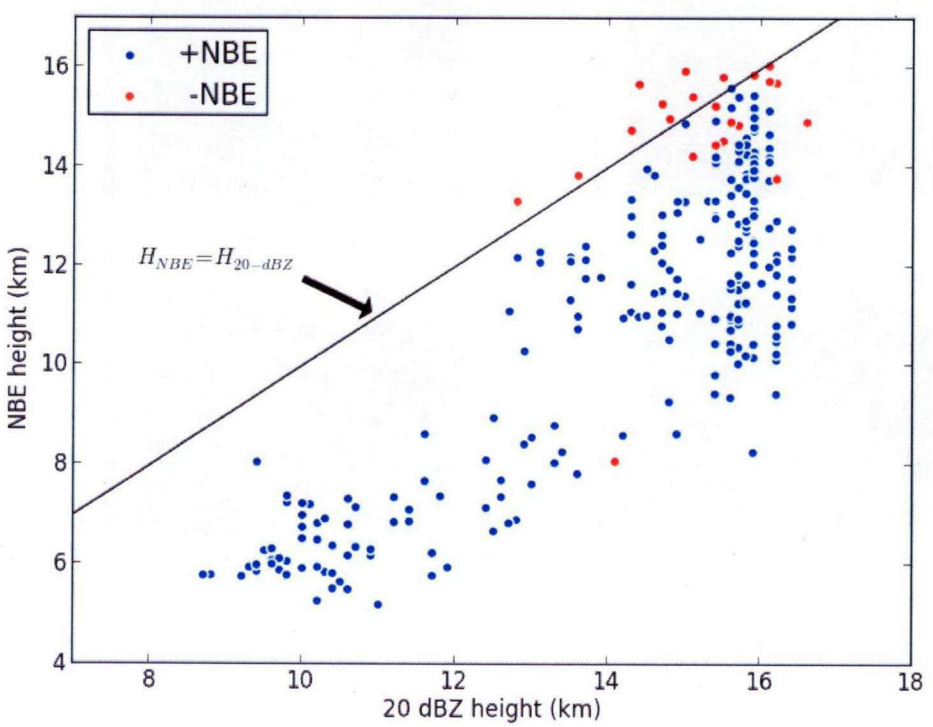

Figure 5.7 Height of all NBEs in this study versus 20-dBZ height of their parent thunderclouds. At the black line, NBE height equals 20-dBZ height.

By comparing discharge heights of NBEs in Osaka (Figure 5.7) with those in China (Figure 4.5), we can see that NBEs in Osaka are much lower than those in China. The difference for –NBEs is especially large. In Osaka, the highest NBE is only 16.0 km while the one in China is 19.9 km and most of –NBEs in China are higher than 16 km. Such difference is probably due to much lower vertical extent of thunderstorms in Osaka. Thunderstorms extending up to 15 km are quite rare in Osaka, and these thunderstorms produced several –NBEs. In China, such thunderstorms are probably more frequent and their vertical extents are also much larger, resulting in more frequent and higher –NBEs. In conclusion, –NBEs are produced at the cloud top of some very vigorous thunderstorms. As the thunderstorm grows higher, the discharge height of –NBE also becomes higher.

Chapter 6

Discussions

6.1 Does winter thunderstorm produce NBE?

Lightning discharges produced in winter thunderstorm in Japan has been widely known for their special features. For example, cloud-to-ground lightning lowering positive charge constitutes a much higher percentage in winter thunderstorm than in summer thunderstorm [*Brook et al.,* 1982]. Bipolar flashes [*Narita et al.,* 1989] and upward flashes [*Saito et al.,* 2009] occur more frequently in winter thunderstorm. Electric field change waveforms produced by return stroke (RS) in winter thunderstorm also shows different fine structures [*Ishii and Hojo,* 1989]. It is currently unclear whether winter thunderstorm can produce NBE. During our observations in Hokuriku during the winter of 2010-2011, we failed to find any NBE. It seems that winter thunderstorm cannot produce NBE. However, we observed a type of special large bipolar pulse that shares some similarities with NBE and yet different from NBE. Such special bipolar pulse is also different from normal bipolar pulse of regular intracloud discharges in that it is apparently not associated with any other discharge processes. Therefore we name it as "isolated large bipolar pulse" (ILBP). We have recorded 14 ILBPs in this observation. In this section I will analyze waveform characteristics of ILBP and compare it with NBE.

Figure 6.1 shows a typical waveform of ILBP in both 1 second and 1 millisecond time scales. Such waveform is different from various types of pulses produced by lightning discharges. First, ILBP is different from radiation waveforms produced by regular intracloud discharge processes as shown by *Weidman and Krider* [1979]. Pulses of regular intracloud discharges usually have much more complex fine structures with small pulses superimposed on the initial half cycle while ILBPs shows simple and smooth change. Second, ILBP is different from bipolar pulses of initial breakdown in that initial breakdown pulses always form pulse trains lasting on the order of 1 ms [*Brook et al.,* 1982; *Ushio et al.,* 1998] while ILBP appears as a single pulse not associated with any other discharge processes. Third, ILBP is also different from NBE. For NBE, peak magnitude of initial polarity is usually much larger than that of overshoot [*Smith et al.,* 1999] while for ILBP, peak magnitudes of two polarities are quite close.

ILBP is sometimes followed by a small pulse about several hundred microseconds later

as shown in Figure 6.1. Such small pulse is produced by ionospheric reflection of radiation signal of ILBP. Contrarily, NBE is usually followed by two reflection pulses as analyzed in section 3.3. The first one is produced by NBE signal reflected from the ionosphere and the second one is produced by the NBE signal first reflected by the ground and then by the ionosphere. The fact that ILBP only has one reflection pulse indicates that its source height is quite close to the ground as is a common situation for lightning discharges in winter thunderstorm.

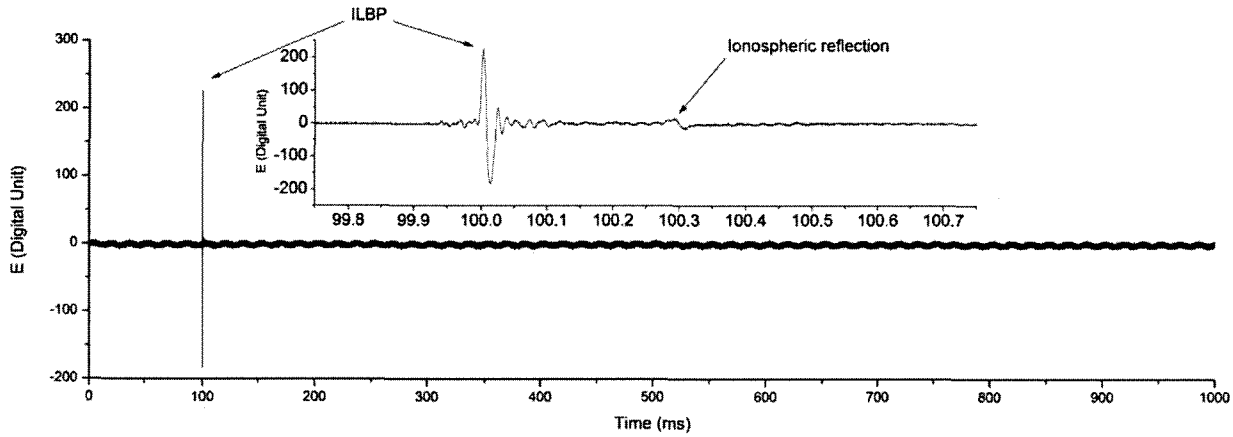

Figure 6.1. Typical waveform of ILBP shown in both 1 second and 1 millisecond scale.

One important feature of ILBP is that its positive and negative peak amplitudes are quite close. The ratio of the main positive peak to the negative peak is in the range of 0.9~1.3 with a mean value of 1.14, indicating amplitudes of positive and negative ends are generally similar with each other. By comparison, NBE usually has much larger initial peak amplitude than its overshoot amplitude. The ratio of initial peak amplitude to overshoot amplitude of NBE is on average 8.8 for 18 NBEs and 9.1 for 6 NBEs as reported by *Willett et al.* [1989] and 2.7 for 24 NBEs as reported by *Smith et al.* [1999]. In fact, the initial positive half cycle and the negative half cycle of ILBP are symmetrical to some extent. Not only do they have close peak amplitudes, but they also have similar pulse widths. Such feature is not common for waveforms produced by lightning discharge processes.

Pulse width of ILBP is mainly between 7~19 μs with a mean value of 12.6 μs. This is generally larger than the pulse width of NBE. Pulse widths of NBEs reported by *Le Vine* [1980] were less than 10 μs. In some studies, only waveforms with pulse width of less than 7 μs were identified as NBE [*Wu et al.,* 2011]. On the other hand, pulse widths of ILBPs are generally smaller than that of RS. The zero-crossing time of radiation field produced by RS is on average 49 μs in Sweden and 89 μs in Sri Lanka as reported by *Cooray and Lundquist* [1985] and 54 μs in Florida as reported by *Lin et al.* [1979]. *Ishii and Hojo* [1989] reported that zero-crossing time of RS in winter is smaller, with mean values of 40 μs for –RS and 93

μs for +RS. As a result, pulse width of ILBPs is generally larger than that of NBEs and smaller than that of RSs.

ILBPs also tend to be temporally isolated with other lightning discharge processes. In other words, ILBP tends to occur as an independent and probably complete discharge event. I could only find one ILBP that seems to be associated with other lightning processes as shown in Figure 6.2. Due to lack of location information, I am not able to confirm whether the ILBP is truly related with the following discharge processes. It is also possible that they are actually independent discharge processes coincidentally occurring within small time intervals. The characteristic of temporal isolation of ILBP is also similar with NBE, which is usually found isolated with other discharge processes but sometimes also appears as the initiation process of regular intracloud discharge (section 3.2).

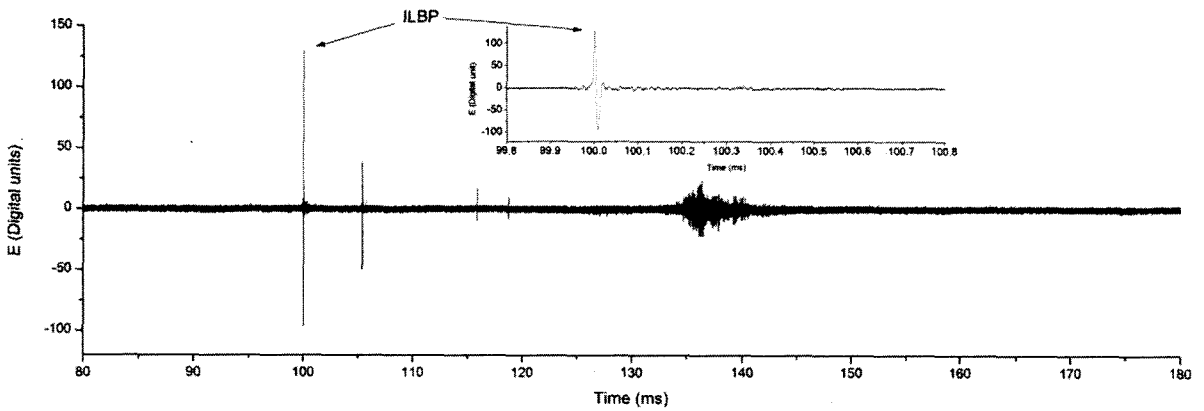

Figure 6.2 An ILBP followed by other discharge processes shown in both 100 ms and 1 ms scale.

ILBP is similar with NBE in several respects, but at the same time, it is also largely different from NBE. Both of ILBP and NBE produce very large electric field changes that are comparable or even larger than that of RSs. And both of them are usually isolated with other discharge processes. On the other hand, pulse width of ILBP is generally larger than that of NBE. For ILBP, the positive and negative peak magnitudes are usually almost the same and two polarities are symmetrical to some extent, but for NBE, the initial peak magnitude is usually much larger than the overshoot peak magnitude. Both polarities of NBEs are frequently observed, while only one polarity of ILBPs has been observed.

According to its polarity (positive as in atmospheric sign convention), ILBP should be produced below the main negative charge layer of a thunderstorm. However, it is unclear whether ILBP is produced between the main negative charge layer and the lower positive charge layer or it is connected with the ground as –RS. If it is a type of intracloud discharge, it may be a special version of NBE in winter thunderstorm. Summer thunderstorms frequently produce NBE, but we could not find any NBE in winter thunderstorm. Perhaps the processes producing NBE in summer thunderstorm, with some special meteorological conditions of

winter thunderstorm, result in ILBP. After all, ILBP and NBE share certain similarities. To further examine this hypothesis, VHF observation of ILBP should be carried out. NBE produces extremely strong VHF radiation, and it would be very interesting to know whether ILBP produces strong VHF radiation.

6.2 Height threshold for NBE production

When comparing distributions of NBE discharge height in Guangzhou and Chongqing (Figure 4.5), it is interesting to note that height distributions of –NBEs are almost the same, while that of +NBEs are largely different in these two regions. Average heights of –NBEs in these two regions are also very close, while that of +NBEs differ by more than 2 km (Table 4.1). It seems that large number of +NBEs cluster below 10 km in Chongqing, while +NBEs in Guangzhou distribute relatively evenly between 9 and 15 km.

Another difference worth noting is that the percentage of –NBE is much larger in Guangzhou than in Chongqing. The number of –NBEs in Guangzhou is about half of the number of +NBEs, while that in Chongqing is only about one fifth of +NBEs. According to the conclusion in section 5.1 that percentage of –NBE increases as convective strength of the thunderstorm increases, it seems that thunderstorms in Guangzhou have stronger convection than that in Chongqing. This can also be inferred from frequencies of –RS in these two regions. In Guangzhou, 138,148 –RSs were detected in 19 days, equivalent to 7271 –RSs per day. In Chongqing, 174,756 –RSs were detected in about two months, equivalent to about 2913 –RSs per day, much smaller than that in Guangzhou. From another perspective, I compared 50 largest hourly rates of total discharge events and –RSs in Guangzhou and Chongqing. In Guangzhou, the 50 largest hourly rates of total discharge events range from 22215 to 3203 counts per hour, much larger than that in Chongqing, which range from 2410 to 1288 counts per hour. The 50 largest hourly rates of –RSs in Guangzhou range from 5826 to 853 counts per hour, also larger than that in Chongqing, which range from 1437 to 776 counts per hour. Given the fact that the lightning detection network in Chongqing has more observation stations and covers larger area than that in Guangzhou (see section 2.1), it should be concluded that thunderstorms are generally more vigorous in Guangzhou than in Chongqing.

Combining these two differences, we speculate on a possible explanation. It is likely that –NBEs can only be produced above certain height. When the charge layers responsible for –NBE production are lifted above certain height, –NBEs can be produced, otherwise –NBEs can rarely occur. Such "critical height" is around 15 km according to the result of this study. Since thunderstorms in Chongqing are generally less vigorous than that in Guangzhou, thunderclouds in Chongqing are generally lower and the upper charge layers have less chance

to develop above the critical height, resulting in much smaller percentage of –NBEs in Chongqing. Normally the middle charge layers responsible for +NBE production are also lower in Chongqing than that in Guangzhou, so +NBE discharge heights in Chongqing are also lower. However, because of the limitation imposed by the "critical height", discharge heights of –NBEs are almost the same in Chongqing and Guangzhou; the difference is that –NBE percentage is much smaller in Chongqing because thunderclouds in Chongqing have less chance to develop to the critical height.

The higher the upper charge layers are lifted above the critical height, the larger chance –NBEs can be produced. However, it is difficult for thundercloud tops to penetrate the tropopause. Competition of such two limitations results in distribution peak between 17 and 18 km for –NBE discharge height. +NBE production should also have a critical height, which is possibly around 7 km. The upper limit for the height of middle charge layers responsible for +NBE production seems to be around 17 km, so +NBEs can occur between 7 km and 17 km, much larger a range than that of –NBEs. Therefore +NBEs have the "space" to show large difference in height distributions in two regions. However, although average discharge heights of +NBEs in two regions differ by more than 2 km, the minimum values only differ by 0.6 km, indicating a lower height limit for +NBEs. The minimum discharge heights of –NBEs in these two regions are also very close (14.6 km and 14.1 km, see discussion in section 4.3), supporting our hypothesis.

Under this hypothesis, –NBE will rarely occur between the lower positive charge layer and the main negative charge layer (Figure 4.6), because these charge layers have very little opportunity to be lifted above the critical height of –NBE (around 15 km). This also results in the fact that –NBEs are usually much fewer than +NBEs, because it is much easier for charge layers responsible for +NBE production to reach the critical height.

Such a hypothesis indicates an initiation mechanism of NBE in which there is energy injecting into thunderclouds from space. The higher a thundercloud develops, the larger energy it receives, and the larger chance there is that NBEs can be produced. Such notion is also consistent with the phenomenon that –NBEs are usually more powerful than +NBEs [*Wu et al.,* 2011]. A possible candidate for such mechanism is runaway breakdown mechanism [e.g., *Roussel-Dupre and Gurevich,* 1996] and likely included with relativistic feedback to increase multiplication of energetic electrons [*Dwyer,* 2003]. In such mechanism, cosmic ray particles play a critical role. There are also some studies trying to relate runaway breakdown mechanism to NBE phenomenology [*Gurevich and Zybin,* 2004; *Gurevich and Zybin,* 2005], but details are still missing to account for differences between +NBE and –NBE.

If our hypothesis is true, a direct result is that NBEs will not be produced in some regions where thunderstorms are lower as illustrated in Figure 6.3. It shows as the latitude increases, the height of tropopause decreases, which sets a limitation on the development of

thunderstorms. When the charge layers responsible for production of NBEs cannot develop above the critical height, NBEs will not be produced. Such mechanism is in accordance with some observations. Lu et al. [2012] reported that their observation in northeast China (51°N) only recorded +NBE without any –NBE. Sharma et al. [2011] reported that no NBE was observed in Sweden (59.8°N, 17.6°E). And our observation result in winter thunderstorm (section 6.1) agrees with this mechanism, because winter thunderstorm is very low so charge layers cannot reach the critical height for NBE production.

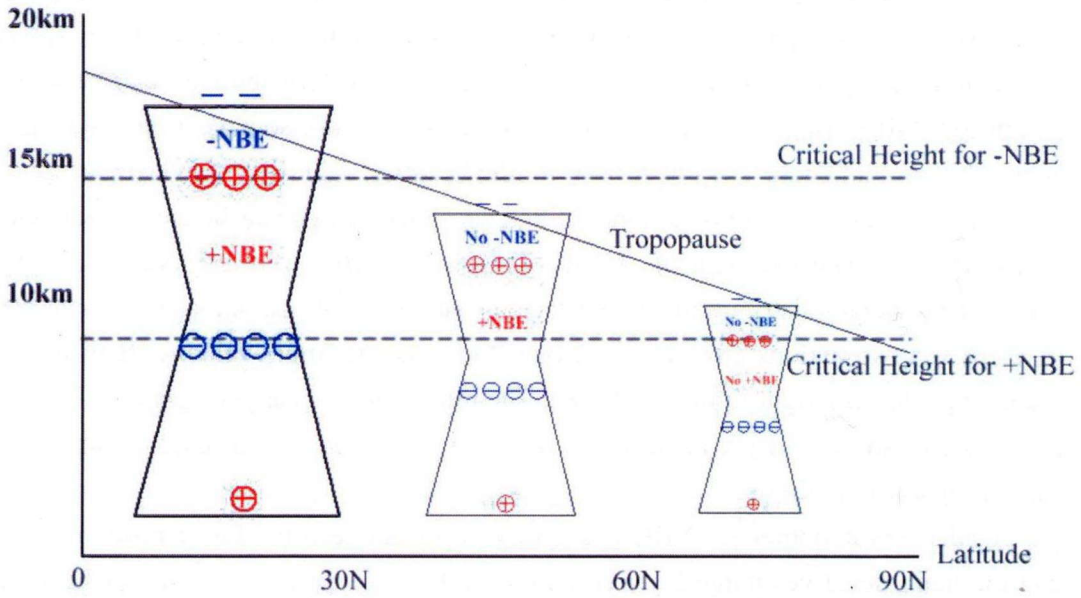

Figure 6.3 Illustration of "critical height" hypothesis and production of NBE in different latitudes.

Our observation in Osaka region (section 5.2) is also consistent with such hypothesis, especially for –NBE. Discharge heights of –NBEs in this study range from 13.3 to 16.0 km (except of the especially low one), and most of them are between 14 and 16 km. Such distribution resembles the lower tail of the distributions in Guangzhou and Chongqing of China (see Figure 4.5). In Osaka region, thunderstorms with cloud top of higher than 15 km are very rare (the PAR is only designed for observation of up to 15 km). Most thunderstorms in Osaka region only developed to around 12 km or even lower, and no –NBEs were produced. Cloud tops of some rare cases analyzed in section 5.2 exceeded the critical height and produced several –NBEs. The highest –NBE is only 16.0 km in this study, compared with larger than 16 km for majority of –NBEs in south China, which is also a manifestation of much lower storm top in Osaka region than that in south China.

6.3 Monitoring severe thunderstorm with NBE

A major question in NBE research is that whether NBE can be used to indicate severe thunderstorm. When analyzing the relationship between NBE and thunderstorm, previous studies usually make no discrimination between positive and negative NBEs, which is probably the reason that the correlation between NBE rate and convective strength is weak. As I have demonstrated in this thesis, there are large differences between +NBE and –NBE, so I suggest that +NBE and –NBE should be discriminated before their relationship with thunderstorm is analyzed. And according to my analysis in Chapter 5, it seems that –NBE is more useful and accurate in indicating the deepest convection.

As analyzed in section 5.2, –NBEs are only produced in the most vigorous thunderstorms (usually higher than 14 km), and –NBEs always occur near the upper boundary of the thundercloud. Therefore, if we can detect –NBE and determine its height, we can estimate the thunderstorm top height right from the –NBE height. Even if we cannot determine NBE height, we can roughly decide the severity of thunderstorm by the presence of –NBE. As long as –NBE is produced, the thunderstorm has probably developed above at least 14 km, which is quite severe. In this way, severe thunderstorms can be conveniently monitored by detecting –NBEs.

I will further analyze two thunderstorm observed in Guangzhou which produced both positive and negative NBEs. I will show the association between production of –NBEs and deep convection.

Observations of a conventional C-band Doppler weather radar is employed here (Figure 2.1). Since radar observations of targets at high altitudes (roughly above 15 km in this dataset) have low resolution reflectivity, making it seriously inaccurate to determine cloud top of higher than 15 km from radar echo top, here I define two quantities to roughly infer storm structures: total volume of reflectivity larger than 30 dBZ (V_{30}) and total volume of reflectivity larger than 30 dBZ above 15 km (V_{30-15}). Two adjacent thunderstorms producing more –NBEs than +NBEs observed in Guangzhou in August 8, 2007 are selected. These two thunderstorms are selected because they are in appropriate distances (between 60 and 100 km) from the radar station; they are close to the lightning location network (less than 120 km), so the location accuracy is high; and they both have clear boundaries, making the analysis easy. Figure 6.4 shows the time series of +NBE rate, –NBE rate and the value of V_{30} and V_{30-15}. Bursts of –NBEs are clearly associated with abrupt increases of V_{30-15}, but V_{30} does not show obvious variation accordingly, indicating that changes of the storms mainly occur above 15 km; that is, the storms are developing higher during the bursts of –NBEs. Although it is so far unclear why variations of V_{30-15} are always several minutes ahead of variations of –NBE rate, the connection between –NBE production and deep convection is obvious, which is also consistent with the finding that a thunderstorm has higher tendency to produce –NBEs as it is more vigorous (section 5.1). It is important to note that in these two cases, 30-dBZ heights are

higher than 15 km when $V_{30-15}>0$, so thundercloud tops are probably comparable to the discharge height of –NBEs in this region (16 to 19 km) during bursts of –NBEs. This phenomenon is also consistent with charge structure in Figure 4.6; when –NBEs are produced, thunderclouds are developing higher, and charge layers are lifted to the height comparable to the discharge height of NBEs. Such thunderstorms are quite severe, so production of –NBE can well indicate severe thunderstorm.

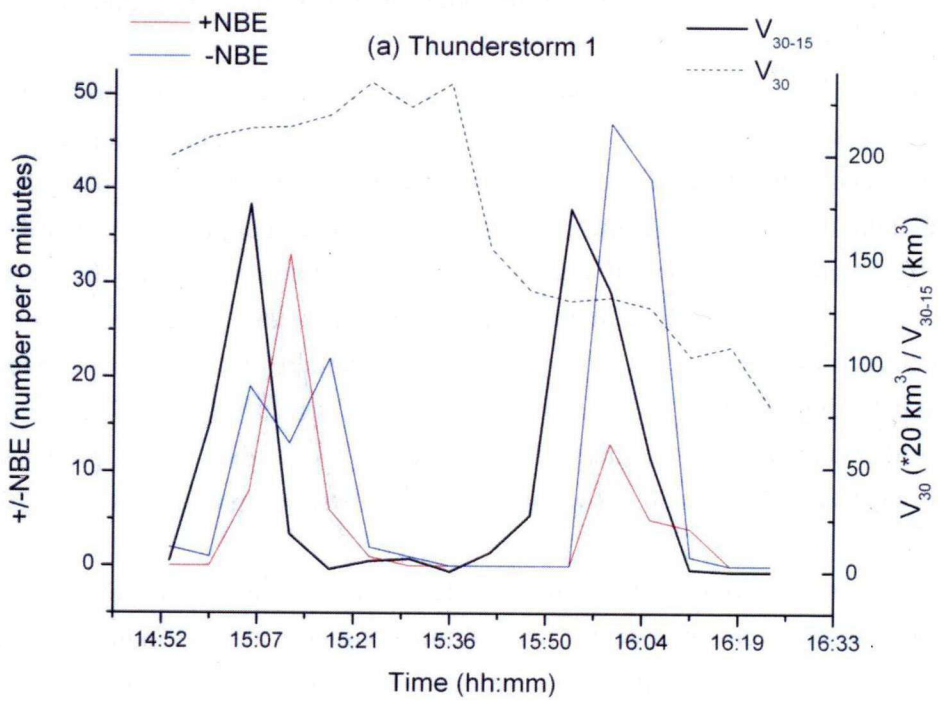

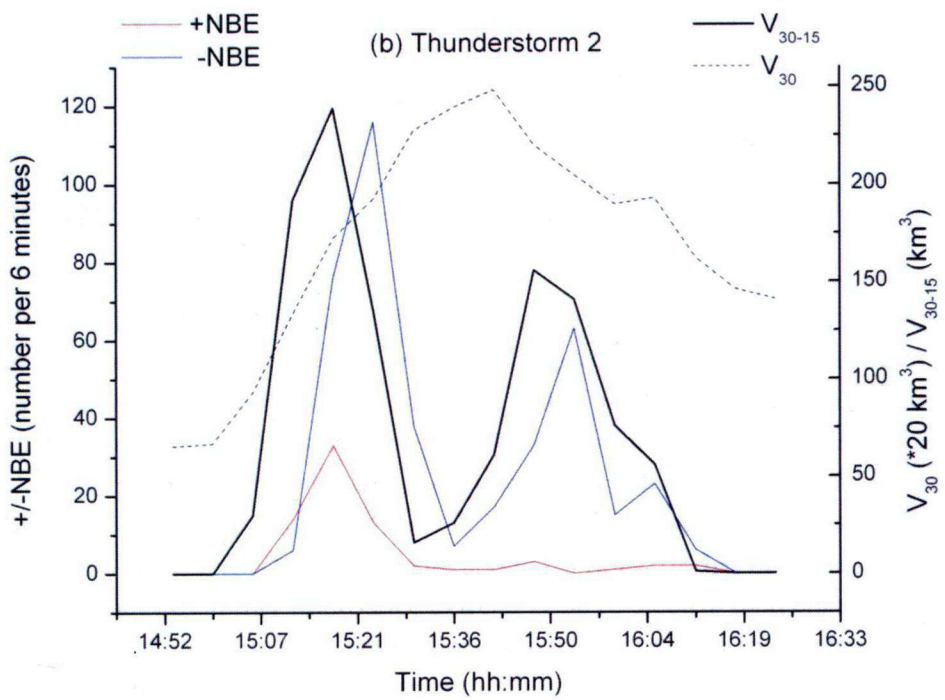

Figure 6.4 Time series of +NBE rate, –NBE rate and the value of V_{30} and $V_{30\text{-}15}$ in two thunderstorms observed in Guangzhou. V_{30} and $V_{30\text{-}15}$ share a scale, but the real value of V_{30} is the scale multiplied by 20.

Chapter 7

Conclusions

This thesis analyzed multiple characteristics of NBE based on observation of NBE in different regions. Because we have recorded large number of both polarities of NBEs, we have the chance to comprehensively compare +NBE with –NBE from different respects. As for the difference between +NBE and –NBE, the major findings are as follows:

1. NBEs generally produce larger electric field changes than –RSs do, and –NBEs are generally more energetic than +NBEs. The normalized peak amplitude of electric field changes produced by –NBEs is on average about 1.6 times of that produced by +NBEs, and –NBEs have higher possibility to produce extremely large electric field changes.

2. NBEs tend to be isolated with other discharge processes, and larger portion of –NBEs than that of +NBEs are temporally isolated with other discharge processes on a timescale of 10 ms.

3. –NBEs mostly occur at higher altitudes than +NBEs do. In Guangzhou and Chongqing of China, most of –NBEs occur between 16 and 19 km, while most of +NBEs occur between 8 and 16 km.

4. –NBEs are generally rarer than +NBEs. Out of 9 storms in Guangzhou, 8 storms produce more +NBEs than –NBEs. But both +NBEs and –NBEs occur in every storm.

5. Considering some short periods that have largest rates of +NBEs or –NBEs, there are significantly larger portion of –NBEs than that of +NBEs occurring in these periods. It indicates that –NBE's occurrences are more temporally compact.

6. The percentage of –NBEs in a given storm has the trend to increase with the convective strength.

These differences are related with each other. First, –NBEs are generally higher than +NBEs (the third difference) and are associated with thunderstorms with cloud top higher than about 14 km. This requires the thunderstorm producing them to be extremely vigorous, which is likely related with the sixth difference. Besides, the region where –NBEs occur probably corresponds to the region between upper positive charge layer and the screening charge layer, where normal lightning discharges can rarely occur, while the region where +NBEs occur is almost the same as the region where normal intracloud discharges occur. This may determine that –NBEs are more temporally isolated with other discharge processes (the second difference).

Since –NBEs are often accompanied by extremely vigorous storms, such vigorous storms usually provide large amount of energy, which may be responsible for –NBE's

energetic discharges (the first difference) and extremely high rates in some short periods (the fifth difference). At the same time, such vigorous state can rarely last for a long time, which makes –NBEs relatively rarer (the fourth difference).

One important result of this thesis is that –NBEs occur at higher altitudes than +NBEs do. Although there are other studies on this issue, my calculation is more accurate and it shows that although many –NBEs can be higher than the tropopause, but extremely high –NBEs (higher than 20 km) are quite unlikely. Based on this result, previous speculation that some NBE might occur as upward discharge above the thunderstorm can be negated.

Analysis of variations of NBE discharge heights in two thunderstorms showed that NBEs can be produced at any position between corresponding charge layers. +NBEs are generally higher when –NBEs are occurring in the same period, and for a given short time period in a single thunderstorm, –NBEs are always higher than +NBEs. This result confirms the charge layer structures for NBE production illustrated in Figure 4.6.

Our observation in Osaka region used PAR for the first time for study of NBE. The PAR observation with high temporal and spatial resolution revealed spatial relationship between NBE and thunderstorm. The result showed that NBEs usually correspond well with the deepest convection, but in some thunderstorms with intense updraft extending above 15 km, +NBEs are produced at the periphery, instead of the center, of the deepest convection. This may be because of decrease of electric field due to elevation of the upper positive charge layer or formation of screening negative charge layer in the region of the deepest convection. +NBEs are usually lower than –NBEs. +NBEs are always produced well inside thundercloud while –NBEs are usually close to the upper boundary of the thundercloud. –NBEs were only produced in a few thunderstorms with the deepest convection while numerous thunderstorms with shallower convection did not produce any –NBE, a phenomenon consistent with "critical height" hypothesis discussed in section 6.2.

Based on these findings, I suggested a way to monitor severe thunderstorms with –NBE. Because –NBEs are only produced in the most vigorous thunderstorms usually higher than 14 km and always occur near the upper boundary of the thundercloud, if we can detect –NBE and determine its height, we can estimate the thunderstorm top height right from the –NBE height. Even if we cannot determine NBE height (as most lightning location systems do), we can roughly decide the severity of thunderstorm by the presence of –NBE. Such a way of monitoring severe thunderstorm is very convenient and has broad implication for thunderstorm remote sensing.

Bibliography

Betz, H.-D., T. C. Marshall, M. Stolzenburg, K. Schmidt, W. P. Oettinger, E. Defer, J. Konarski, P. Laroche, and F. Dombai (2008), Detection of in-cloud lightning with VLF/LF and VHF networks for studies of the initial discharge phase, *Geophys. Res. Lett., 35*, L23802, doi:10.1029/2008GL035820.

Bracewell, R. N., K. G. Budden, J. A. Ratcliffe, T. W. Straker, and K. Weekes (1951), The ionospheric propagation of low- and very low-frequency radio waves over distances less than 1000 km, *Proc. Inst. Electr. Eng., 3*, 221–236.

Brook, M., M. Nakano, P. Krehbiel, and T. Takeuti (1982), The Electrical Structure of the Hokuriku Winter Thunderstorms, *J. Geophys. Res., 87,* 1207-1215.

Cooray, V., and S. Lundquist (1985), Characteristics of the radiation fields from lightning in Sri Lanka in the tropics, *J. Geophys. Res., 90*(D4), 6099-6109.

Dwyer, J. R. (2003), A fundamental limit on electric fields in air, *Geophys. Res. Lett., 30*(20), 2055, doi:10.1029/2003GL017781.

Eack, K. B. (2004), Electrical characteristics of narrow bipolar events, *Geophys. Res. Lett.,* 31, L20102, doi:10.1029/2004GL021117

Fierro, A. O., X. M. Shao, T. Hamlin, J. M. Reisner, and J. Harlin (2011), Evolution of eyewall convective events as indicated by intracloud and cloud-to-ground lightning activity during the rapid intensification of hurricanes Rita and Katrina, *Mon. Weather Rev., 139*, 1492-1504, doi:10.1175/2010MWR3532.1.

Gurevich, A. V., and K. P. Zybin (2004), High energy cosmic ray particles and the most powerful discharges in thunderstorm atmosphere, *Phys. Lett. A, 329*, 341–347, doi:10.1016/j.physleta.2004.06.094.

Gurevich, A. V., and K. P. Zybin (2005), Runaway breakdown and the mysteries of lightning, *Phys. Today, 58*, 37–43.

Hamlin, T., T. E. Light, X. M. Shao, K. B. Eack, and J. D. Harlin (2007), Estimating lightning channel characteristics of positive narrow bipolar events using intrachannel current reflection signatures, *J. Geophys. Res., 112*, D14108, doi:10.1029/2007JD008471.

Hamlin, T., K. C. Wiens, A. R. Jacobson, T. E. Light, and K. B. Eack (2009), Space- and ground-based studies of lightning signatures, in *Lightning: Principles, Instruments and Applications*, edited by Betz, H., U. Schumann, and P. Laroche, *Springer Verlag*, 287-307.

Holden, D. N., C. P. Munson, and J. C. Devenport (1995), Satellite observations of transionospheric pulse pairs, *Geophys. Res. Lett.*, 22(8), 889-892.

Ishii, M. and J. Hojo (1989), Statistics on Fine Structure of Cloud-to-Ground Lightning Field Waveforms, *J. Geophys. Res., 94*, 13267-13274.

Jacobson, A. R. (2003), How do the strongest radio pulses from thunderstorms relate to lightning flashes?, *J. Geohpys. Res., 108*(D24), 4778, doi: 10.1029/2003JD003936.

Jacobson, A. R., and T. E. L. Light (2003), Bimodal radio frequency pulse distribution of intracloud-lightning signals recorded by the FORTE satellite, *J. Geophys. Res.,* 108(D9), 4266, doi:10.1029/2002JD002613.

Jacobson, A. R., and M. J. Heavner (2005), Comparison of narrow bipolar events with ordinary lightning as proxies for severe convection, *Mon. Weather Rev., 133*, 1144-1154.

Kawasaki, Z., R. Mardiana, and T. Ushio (2000), Broadband and narrowband RF interferometers for lightning observations, *Geophys. Res. Lett., 27*, 3189-3192.

Kitagawa, N., and M. Brook (1960), A comparison of intracloud and cloud-to-ground lightning discharges, *J. Geophys. Res., 65*(4), 1189-1201.

Lapp, J. L., and J. R. Saylor (2007), Correlation between lightning types, *Geophys. Res. Lett.,* 34, L11804, doi:10.1029/2007GL029476.

LeVine, D.M. (1980), Sources of the strongest RF radiation from lightning, *J. Geophys. Res., 85*(C7), 4091-4095.

Light, T. E. L., and A. R. Jacobson (2002), Characteristics of impulsive VHF lightning signals observed by the FORTE satellite, *J. Geophys. Res.,* 107(D24), 4756, doi:10.1029/2001JD001585.

Lin, Y. T., M. A. Uman, J. A. Tiller, R. D. Brantley, W. H. Beasley, E. P. Krider, and C. D. Weidman (1979), Characterization of lightning return stroke electric and magnetic fields from simultaneous two-station measurements, *J. Geophys. Res., 84*, 6307-6314.

Liu, H., W. Dong, T. Wu, D. Zheng, and Y. Zhang (2012), Observation of compact intracloud discharges using VHF broadband interferometers, *J. Geophys. Res., 117*, D01203, doi:10.1029/2011JD016185.

Lu, F., B. Zhu, M. Ma, L. Wei, and D. Ma (2012), Observations of narrow bipolar

322 events during two thunderstorms in Northeast China, *Sci. China Earth Sci., 55,* 323 1–12.

Matsui, M., and N. Takano (2010), Evaluation of lightning location accuracy of JLDN with a lightning video camera system. *Asia-Pacific International Symposium on Electromagnetic Compatibility*, 1142-1145.

Nag, A., and V. A. Rakov (2010a), Compact intracloud lightning discharges: 1. Mechanism of electromagnetic radiation and modeling, *J. Geophys. Res.*, 115, D20102, doi:10.1029/2010JD014235.

Nag, A., and V. A. Rakov (2010b), Compact intracloud lightning discharges: 2. Estimation of electrical parameters, *J. Geophys. Res.*, 115, D20103, doi:10.1029/2010JD014237

Nag, A., V. A. Rakov, D. Tsalikis, and J. A. Cramer (2010), On phenomenology of compact intracloud lightning discharges, *J. Geophys. Res., 115*, D14115, doi:10.1029/2009JD012957.

Narita, K., Y. Goto, H. Komuro, and S. Sawada (1989), Bipolar Lightning in Winter at Maki, Japan, *J. Geophys. Res., 94,* 13191-13195.

Qie, X., T. Zhang, C. Chen, G. Zhang, T. Zhang, and W. Wei (2005), The lower positive charge center and its effect on lightning discharges on the Tibetan Plateau, *Geophys. Res. Lett., 32*, L05814, doi:10.1029/2004GL022162.

Riousset, J. A., V. P. Pasko, P. R. Krehbiel, W. Rison, and M. A. Stanley (2010), Modeling of thundercloud screening charges: Implications for blue and gigantic jets, *J. Geophys. Res.*, 115, A00E10, doi:10.1029/2009JA014286.

Rison, W., R. J. Thomas, P. R. Krehbiel, T. Hamlin, and J. Harlin (1999), A GPS-based three-dimensional lightning mapping system: Initial observations in central New Mexico, *Geophys. Res. Lett., 26*, 3573-3576.

Roussel-Dupré, R., and A. V. Gurevich (1996), On runaway breakdown and upward propagating discharges, *J. Geophys. Res., 101*(A2), 2297–2311, doi:10.1029/95JA03278.

Saito, M., M. Ishii, H. Kawamura and T. Shindo (2009), Location of Negative Charge Associated with Continuing Current of Upward Lightning Flash in Winter, *IEEJ Trans. PE, 129*, 929-934.

Shao, X. M., M. Stanley, A. Regan, J. Harlin, M. Pongratz, and M. Stock (2006), Total Lightning Observations with the New and Improved Los Alamos Sferic Array (LASA), *J. Atmosph. And Oceanic Techn., 23*, 1273-1288.

Sharma, S. R., V. Cooray, and M. Fernando (2011), Unique lightning activities pertinent to tropical and temperate thunderstorms, J. Atmos. Sol.–Terr. Phys., 73(4), 483–487, doi:10.1016/j.jastp.2010.11.006.

Smith, D., X. M. Shao, D. N. Holden, C. T. Rhodes, M. Brook, P. R. Krehbiel, M. Stanley, W. Rison, and R. Thomas (1999), A distinct class of isolated intracloud lightning discharges and their associated radio emissions, *J. Geophys. Res., 104*(D4), 4189-4212.

Smith, D.A., K. B. Eack, J. Harlin, M. J. Heavner, A. R. Jacobson, R. S. Massey, X. M. Shao,

and K. C. Wiens (2002), The Los Alamos sferic array: A research tool for lightning investigations, *J. Geophys. Res., 107*(D13), 4183, doi:10.1029/2001JD000502.

Smith, D. A., M. J. Heavner, A. R. Jacobson, X. M. Shao, R. S. Massey, R. J. Sheldon, and K. C. Wiens (2004), A method for determining intracloud lightning and ionospheric heights from VLF/LF electric field records, *Radio Sci., 39*, RS1010, doi:10.1029/2002RS002790.

Stolzenburg, M., W. D. Rust, and T. C. Marshall (1998), Electrical structure in thunderstorm convective regions 3. Synthesis, *J. Geophys. Res., 103*(D12), 14,097–14,108, doi:10.1029/97JD03545.

Suszcynsky, D. M., and M. J. Heavner (2003), Narrow bipolar events as indicators of convective strength, Geophys. *Res. Lett., 30*(17), 1879, doi:10.1029/2003GL017834.

Takayanagi, Y., M. Akita, Y. Nakamura, S. Yoshida, T. Morimoto, T. Ushio, Z. Kawasaki, and K. Yamamoto (2011), Development of VLF/LF Bands Interferometer and its Initial Observations, *IEEJ Trans. FM, 131,* 716-722, doi:10.1541/ieejfms.131.716. (in Japanese)

Ushio, T., Z. Kawasaki, K.Matsuura, and D. Wang (1998), Electric fields of initial breakdown in positive ground flash, *J. Geophys. Res., 103*, 14135-14139.

Weidman, C. D. and E. P. Krider (1979), The Radiation Field Wave Forms Produced by Intracloud Lightning Discharge Processes, *J. Geophys. Res., 84,* 3159-3164.

Watson, S. S., and T. C. Marshall (2007), Current propagation model for a narrow bipolar pulse, *Geophys. Res. Lett.,* 34, L04816, doi:10.1029/2006GL027426.

Wiens, K. C., T. Hamlin, J. Harlin, and D. M. Suszcynsky (2008), Relationships among Narrow Bipolar Events, "total" lightning, and radar-inferred convective strength in Great Plains thunderstorms, *J. Geophys. Res., 113*, D05201, doi:10.1029/2007JD009400.

Willett, J. C., J. C. Bailey, and E. P. Krider (1989), A class of unusual lightning electric field waveforms with very strong high-frequency radiation, *J. Geophys. Res., 94*, 16,255-16,267.

Wu, T., W. Dong, Y. Zhang, and T. Wang (2011), Comparison of positive and negative compact intracloud discharges, *J. Geophys. Res., 116,* D03111, doi:10.1029/2010JD015233.

Yoshikawa, E., T. Ushio, Z. Kawasaki, S. Yoshida, T. Morimoto, F. Mizutani, and M. Wada (2012), MMSE beam forming on fast-scanning phased array weather radar, *IEEE Trans. Geosci. Remote Sens.,* in press, doi:10.1109/TGRS.2012.2211607.

List of Publication

Journal Papers

1. **T. Wu**, Y. Takayanagi, S. Yoshida, T. Funaki, T. Ushio, Z. Kawasaki., "Spatial relationship between lightning narrow bipolar event and parent thunderstorm as revealed by phased array radar", Geophysical Research Letter, doi:10.1002/grl.50112, in publication.

2. **T. Wu**, W. Dong, Y. Zhang, T. Funaki, S. Yoshida, T. Morimoto, T. Ushio, Z. Kawasaki, "Discharge height of lightning narrow bipolar events", Journal of Geophysical Research, 117, D05119, doi:10.1029/2011JD017054, 2012.

3. **T. Wu**, W. Dong, Y. Zhang, and T. Wang, "Comparison of positive and negative compact intracloud discharges", Journal of Geophysical Research, 116, D03111, doi:10.1029/2010JD015233, 2011.

Proceedings of International Conferences

1. **T. Wu**, T. Funaki, S. Yoshida, T. Morimoto, T. Ushio, Z. Kawasaki, "Discharge height of lightning narrow bipolar events and new observation with phased array radar", AGU Fall Meeting 2012, San Francisco, December 2012

2. **T. Wu**, W. Dong, Y. Zhang, T. Funaki, S. Yoshida, T. Morimoto, T. Ushio, Z. Kawasaki, "Discharge height of lightning Narrow Bipolar Events and its relationship with thunderstorms", JpGU International Symposium 2012, Chiba, Japan, May 2012

Others

1. **T. Wu**, T. Takayanagi, T. Funaki, S. Yoshida, T. Ushio, Z-I. Kawasaki, T. Morimoto, M. Shimizu, "Preliminary breakdown pulses of cloud-to-ground lightning in winter", Journal of Atmospheric and Solar-Terrestrial Physics, under review.

2. **T. Wu**, Y. Takayanagi, T. Funaki, S. Yoshida, T. Ushio, Z. Kawasaki, T. Morimoto,

Y. Nakamura, "Isolated large bipolar pulse (ILBP) produced by lightning discharge in winter thunderstorm", IEEJ Transactions on Fundamentals and Materials, under review.

3. H. Liu, W. Dong, **T. Wu**, D. Zheng, Y. Zhang, "Observation of compact intracloud discharges using VHF broadband interferometers", Journal of Geophysical Research, 117, D01203, doi:10.1029/2011JD016185.